การศึกษาโคโรนาดิสชาร์จที่ถูกเหนี่ยวนำโดยอนุภาคในระบบฉนวน

นายจอมรง อู

วิทยานิพนธ์นี้เป็นส่วนหนึ่งของการศึกษาตามหลักสูตรปริญญาวิศวกรรมศาสตรมหาบัณฑิต

สาขาวิชาวิศวกรรมไฟฟ้า ภาควิชาวิศวกรรมไฟฟ้า

คณะวิศวกรรมศาสตร์ จุฬาลงกรณ์มหาวิทยาลัย

ปีการศึกษา 2559

Study on Particle-Induced Corona Discharge in Insulation Systems

Mr. Chomrong Ou

A Thesis Submitted in Partial Fulfillment of the Requirements
for the Degree of Master of Engineering Program in Electrical Engineering
Department of Electrical Engineering
Faculty of Engineering
Chulalongkorn University
Academic Year 2016

Thesis Title	Study on Particle-Induced Corona Discharge in Insulation Systems
By	Mr. Chomrong Ou
Field of Study	Electrical Engineering
Thesis Advisor	Professor Boonchai Techaumnat, Ph.D.

Accepted by the Faculty of Engineering, Chulalongkorn University in Partial Fulfillment of the Requirements for the Master's Degree

....Dean of the Faculty of Engineering

(Associate Professor Supot Teachavorasinskun, D.Eng.)

THESIS COMMITTEE

....Chairman

(Assistant Professor Komson Petcharaks, Ph.D.)

....Thesis Advisor

(Professor Boonchai Techaumnat, Ph.D.)

....External Examiner

(Nutthaphong Tanthanuch, Ph.D.)

จอมรง อู : การศึกษาโคโรนาดิสชาร์จที่ถูกเหนี่ยวนำโดยอนุภาคในระบบฉนวน (Study on Particle-Induced Corona Discharge in Insulation Systems) อ.ที่ปรึกษาวิทยานิพนธ์หลัก: บุญชัย เตชะอำนาจ, 61 หน้า.

ระบบฉนวนก๊าซเป็นระบบที่นิยมใช้อย่างแพร่หลาย เนื่องจากความน่าเชื่อถือในการทำงาน, ความปลอดภัย และใช้พื้นที่น้อย. อนุภาคตัวนำในระบบฉนวนก๊าซเป็นสาเหตุหนึ่งที่ทำให้เกิดความผิดพร่องขึ้นในระบบฉนวนก๊าซ. วัตถุประสงค์ของการศึกษาครั้งนี้ เพื่อตรวจสอบคุณลักษณะการเกิดโคโรนาดิสชาร์จอันเป็นผลจากอนุภาคที่มีรูปทรงของส่วนปลายที่แตกต่างกัน ภายใต้เงื่อนไขของช่องว่างระหว่างอนุภาคและอิเล็กโทรดค่าต่างๆ. การทดลองดำเนินการในสองลักษณะ ได้แก่ (1) อนุภาคมีส่วนปลายกลมมน, ปลายแหลมตัดเฉียง และปลายแหลมคมหรือลักษณะทรงคล้ายทรงกลม. อนุภาคตั้งตรงขึ้นตามแนวดิ่งและปลายอีกด้านสัมผัสกับอิเล็กโตรดกราวนด์. (2) อนุภาคมีส่วนปลายแหลมตัดเฉียงหรือปลายระนาบ โดยอนุภาคถูกแขวนลอยอยู่ตามแนวดิ่งโดยมีระยะห่างระหว่างอนุภาคกับอิเล็กโตรดกราวนด์. การศึกษานี้ยังใช้วิธีการวิเคราะห์ เพื่อการประมาณค่าแรงดันเริ่มเกิดโคโรนาตามกลไกการเกิดเบรกดาวน์แบบสตรีมเมอร์. สำหรับในกรณีที่อนุภาคตั้งตรงในแนวดิ่งและสัมผัสกับอิเล็กโตรดกราวนด์ แรงดันการเริ่มเกิดโคโรนามีค่าสูงขึ้นเมื่อส่วนปลายของอนุภาคมีลักษณะเป็นปลายแหลม. ขนาดของกระแสไฟฟ้าจากการเกิดดิสชาร์จบางส่วนและประจุมีแนวโน้มเพิ่มขึ้น เมื่อแรงดันเริ่มเกิดโคโรนามีค่าสูงขึ้น. ประจุจากการเกิดดิสชาร์จบางส่วนเป็นไปในแนวทางเดียวกันกับค่าที่ได้จากการวัด. ในการทดลองกรณีที่อนุภาคลอยตัวไม่สัมผัสกับอิเล็กโตรดกราวนด์ อนุภาคที่มีส่วนปลายเป็นระนาบตรงจะเกิดการเบรกดาวน์ เมื่อระยะห่างระหว่างอนุภาคกับอิเล็กโตรดกราวนด์เท่ากับ 0.25 มิลลิเมตร ถึง 1 มิลลิเมตร และจะเกิดโคโรนาดิสชาร์จเมื่อระยะห่างดังกล่าวเพิ่มขึ้นเป็น 1.5 มิลลิเมตร ถึง 2 มิลลิเมตร. แรงดันการเริ่มเกิดโคโรนา, ขนาดของกระแส และประจุจะขึ้นอยู่กับระยะห่างระหว่างอนุภาคกับอิเล็กโตรดกราวนด์ และลักษณะของส่วนปลายของอนุภาค.

ภาควิชา	วิศวกรรมไฟฟ้า	ลายมือชื่อนิสิต	....
สาขาวิชา	วิศวกรรมไฟฟ้า	ลายมือชื่อ อ.ที่ปรึกษาหลัก	....
ปีการศึกษา	2559		

5770515421 : MAJOR ELECTRICAL ENGINEERING
KEYWORDS: GAS INSULATED SYSTEMS, PARTICLE,CORONA,PARTIAL DISCHARGE AND PD CHARGE

CHOMRONG OU: Study on Particle-Induced Corona Discharge in Insulation Systems. ADVISOR: PROF. BOONCHAI TECHAUMNAT, Ph.D., 61 pp.

Gas insulated systems are in popular use for operational reliability, safety, and compactness. Metallic particles in gas insulation systems are a common source of failures. The objective of this study is to investigate the characteristic of corona discharge induced by particles having different ending shapes with various gaps between the particle and the electrode. The experiments are conducted with two configurations, (i) particles having rounded, sharp, very-sharp tips or spheroidal particle are set to stand in contact with the grounded electrode, (ii) particle having sharp or flat tips are set to float above the, grounded electrode by small gaps. An analysis is also applied to study. The corona inception voltage is estimated by using streamer breakdown criteria. For the experiment on the standing particles, the corona inception voltage is higher with sharper particle tip; and partial discharge current magnitude and charge tend to be higher or larger for higher corona inception voltage. The partial discharge charge follows the tendency of the measured values for the standing particles. For the experiment on the floating particles, the particles having flat upper tip yield direct breakdown at 0.25 to 1 mm, and corona discharge at larger gap from 1.5 to 2 mm. The corona inception voltage, current magnitude and charge depend on the gap lengths and the tip shapes of the particles.

Department:	Electrical Engineering	Student's Signature	....
Field of Study:	Electrical Engineering	Advisor's Signature	....
Academic Year:	2016		

ACKNOWLEDGEMENTS

This thesis could not have been completed without great supports and guidance from precious people over two years. I give acknowledgment to Professor Kunihiko Hidaka for his comments and some of experimental materials.

I greatly appreciate Assistance Professor Komson Petcharaks, Doctor Nutthaphong Tanthanuch, my thesis committees, for valuable comments on my work. They share useful ideas to improve quality of my thesis. I express thank to Assistant Professor Weerapun Rungseevijitprapa, Supatana Auethavekiat, and Doctor Channarong Banmongkol for providing me the constructive courses.

I am sincerely grateful to Doctor Long Bun and Mister Piseth Sean, Department of Electrical and Energy, Institute of Technology of Cambodia, for their external supports and coordination during my study.

I am grateful to Mister Nitipong Panklang, Tatchawin Sangsri, Monekham Vilaisient and Teera Kriengkriwut for their technical help and discussion on my works. I also thank Mister Thavorn Auedee, and Kriengkrai Odthanu for preparing experimental equipment and solving the technical problem.

I gratefully acknowledge the ASEAN University Network/Southeast Asia Engineering Education Development Network (AUN/SEED-Net) and Thailand Research Fund for their financial supports. I give my gratitude to the staffs and the International School of Engineering (ISE), Chulalongkorn University for their cares and helps during my study.

At the end, I wish to thank my family and friends who always inspirit and care me during my study.

CONTENTS

Page

Page

LIST OF FIGURES

LIST OF TABLE

CHAPTER I

INTRODUCTION

1.1 General introduction

Continuous electrical supply with reliability, safety and stability to users is a main aim of electrical utilities. For the rapid growing of power consumption and long transmission, high voltage (HV) is used to reduce power loss and voltage drop, etc. Electrical insulation systems play an important role in high voltage engineering to protect high voltage equipment from electrical stress [1]. Gases are used in insulation systems to insulate the HV conductor from ground. Sulfur hexafluoride (SF_6), air and vacuum are in popular use for insulation systems. They are nontoxic and noncorrosive. They can reduce heat, and enhance stability of dielectric coefficient with low dielectric loss [2]. Basically, gases used in insulation systems are required to prevent partial discharge or breakdown with high electric strength. Air is naturally used for overhead transmission lines, but it has a limit in dielectric strength under atmospheric pressure. Therefore, compressed gases are used to provide superior insulation [3]. For example, SF_6, which also has excellent arc extinguishing, is used for circuit breakers[4].

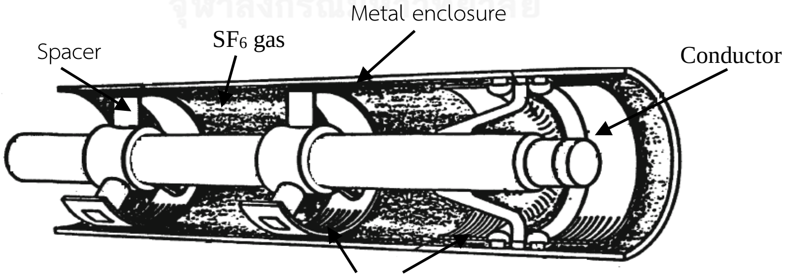

Figure 1.1 Typical design of GIS [5].

Figure 1.1 shows a typical design of gas insulation switchgears (GIS). The conductor is mainly insulated by SF_6 and completely sealed in a metal enclosure. The grounded enclosure also protects human from electric-shock hazard caused by a fault inside GIS. For substations in city, which have limited space, GIS optimize constructional space compared to conventional air insulated systems. GIS also suppress power loss, and reduce the electromagnetic noise due to partial discharge.

Although GIS provide an excellent insulation, it has been reported that the existence of particles is a major cause of insulation failures [6]. The particles may be present in a gas insulated system by various means during fabrication, maintenance, or mechanical operation. Electric field distribution is distorted when particles exist in GIS vicinity. The particles usually intensify electric field near their surfaces due to the higher dielectric constant or conductivity than the gas dielectrics [7]. Excessively strong electric field may result in partial discharge in the gas medium, which has a critical effect on the breakdown of the insulation system. Additionally, conductive particles are charged when they are in contact with another conductor under an electric field. The charged particles can be moved by the force inserted from electric field. The movement of particles possibly promotes the harmful effect of the particle on the insulating performance, in particular, when the particles are attracted closer to an energized electrode.

When partial discharge occurs, it may be observed by its luminous and audible phenomena initiating in highest electric field region [8]. The partial discharge causes electrical power losses. The mechanical degradation is also caused by corona discharge due to material erosion [9]. The degree of damage depends on the type of insulation systems and magnitude of the discharge.

1.2 Literature reviews

In actual insulation systems, particles have a diversity of shapes and dimensions. In experiments, spherical and wire particles with various dimensions are used to represent the actual particles. The particles are set in contact with or float above the grounded electrode in compressed air or SF_6. Under influence of electric field, the particles are charged and moved by electrostatic force. The movement of particles promotes partial discharge. The related studies can be classified into (i) the particle motions (ii) the discharge initiated by particles (iii) the particle motion manipulation. In addition, numerical calculations based on the streamer breakdown criteria are also applied to find an agreement between experimental and analytical values.

1.2.1 Particles motions

When a particle is placed on a grounded electrode under nonuniform electric field, it may lift to the upper electrode by electrostatic force when the force is greater than the particle weight. The particle is found to stand before lifting because of electrostatic torque [10].

Viet et. al. analyzed the behavior of electric field, induced charge and electrostatic force on spheroidal particles [11]. The particles were set to be in contact with or floated above the grounded electrodes under external electric field. For the particle standing on the ground electrode, the electric field was highest at the top pole of spheroidal particle, and decreased to zero at the bottom pole. The electric field was higher when the ratio of the major-to-minor axis became larger. Approximately 80% of net charge and electrostatic force were distributed on the upper haft of the particle. When an uncharged particle was floated above the grounded electrode, the maximal field was at the bottom pole of particle. The electric field increased when the ratio of major axis of particle to gap increased.

Sakai et. al. [12] studied the particle behavior under AC voltage between non-parallel electrodes in air. The upper electrode was tilted to make an angle 3.5° with the lower electrode. The particles were stainless-steel and aluminum wires having diameter of 0.5 and length of 1.0 mm. They were initially placed at the right side of the grounded electrode, where the gap between electrodes was highest. When 10 kV, 60 Hz AC voltage was applied to the electrode, the particles lifted at initial position. They lifted, but did not across full gap between electrodes. They also bounced on grounded electrode, and tended to reach higher field region causing breakdown. When the frequency was increased to 500 Hz, and the particles lifted across the gap and bounced forward to high field. The bouncing was more stable than that in case of 60 Hz.

1.2.2 Corona induced by particles

Experiments were performed to explain the behavior of corona discharge initiated by particle. Kudo et. al. observed corona induced by hemispherical-end wire particles floated in a parallel electrode system with 10 or 20 mm air gap [13]. The particles had 0.25 mm diameter and 6–12 mm length. The results showed that the corona onset voltage depended on the length and position of particles. The corona onset voltage was higher for shorter particle. When the particle was in contact with the negative electrode, the corona onset voltage was smallest. The corona onset voltage increased with the gap distance from the bottom of particle to the grounded electrode up to 0.8 mm, and kept almost constant when the gap was longer than 0.8 mm. When the particle was in contact with the positive electrode, the positive corona discharge occurred stably. The corona onset voltage of the particle at positive electrode was slightly larger than that at the negative electrode.

Asano et. al. investigated bipolar corona discharge induced by filamentary particles in parallel electrodes with 20 mm air gap [14]. The particles were copper wires with perpendicularly cut ends. They had 0.25 mm diameter and 4–10 mm length. The authors reported that the corona onset voltage did not depend on gap for the particle length of 4 or 6 mm. The corona onset voltage slightly depended on the particle length. When the particle length increased, the corona onset voltage decreased. They also increased the applied voltage until breakdown took place. The breakdown voltage was higher with increasing gap.

Negara et. al. extensively studied the corona phenomena initiated by floating spheroidal particles in air or SF6, compressed in a chamber. The negative or positive DC voltages was applied to a planar electrode system [15]. The particles had a 10 mm major axis and 1 mm minor axis. The electrodes were separated by 45 mm from each other. They found that the corona pulses in SF_6 regularly appeared in time as in air. The positive and negative coronas from both tips of particle were difficult to be discriminated by only observing of corona currents, as the currents pulses appeared as a mixture of positive and negative coronas. When the particles were close to either electrode, the amplitudes of corona current pulses were large with high repetition rate of current pulses. When the particles were placed away from the electrode, the corona and breakdown hardly occurred with increasing voltage, compared to air. The negative corona took place more easily than the positive corona. The repetitions of negative and positive pulses in time were independent of particle position for both positive and negative applied voltages.

Morcos et. al. studied particle-initiated corona and breakdown in gas insulation transmission line [16]. The particles with hemispherical ends had length of 2, 4 and 6.4 mm and diameter of 0.45 mm. They were placed in a 70 or 190 mm diameter coaxial electrode arrangement filled with SF_6 compressed up to 0.2 MPa. Three levels of AC voltages with 60 Hz applying to the coaxial system were 120, 140 and 170 kV. The results showed that the corona onset and the breakdown voltages increased with higher gas pressure. The higher applied voltage increased corona current magnitude, but reduced the repetition rate of pulses.

1.2.3 Particle motion manipulation

Excluding particles from GIS is impossible. Therefore, many techniques are proposed to eliminate the effect of the corona initiated by particles in GIS. Dielectric coating reduced the effect of particle contamination[17]. The conductors and the enclosure were coated by a dielectric material to prevent the particles from contact charging. The coating dielectric impeded the development of pre-discharge. Once the particles were lifted under electric field, they collided with the coated conductor or enclosure, the charge of particle reduced (compared to the case without coating). Then, the discharge hardly occurred. Although this technique provided a better solution, the possibility of discharge still remained. To reduce possibility of discharge further, electrostatic particle trap was designed to trap and contain the particles [18]. The particle trap is located at the bottom enclosure where the electric field is low. When the particles moves to the vicinity of the particle trap, they were attracted to slot edge of the trap. Once trapped, the particles no longer moved, reducing possibility of discharge.

Khan et. al. studied the motion behavior of particle near three types of acrylic spacers in air [19]. The experiment was carried out by using stainless steel sphere with radius of 0.5 mm and wire particles having length of 2–3 mm and diameter of 0.25 and 0.5 mm. The spacers were trapezoidal, inclined, and cone and rib sharps, as shown in Figure 1.2. Their lengths were of 80 mm. The upper electrode was tilted with angle θ = 3.5°. The authors found that the particles moved to the higher electric field region and lifted to adhere the spacers even when the applied voltage was low. They suggested that the spacer angle φ should be between 150° and 90° to eliminate the effect of particle motion. For the larger angle φ, the particles easily moved away from the spacer at lower on set motion voltage, and hardly lifted with low applied voltage. When the particles made a contact with the spacer, they hardly adhered to the spacer. The particles were pulled out from the spacer due to electrostatic repulsion between the charge on the particle and the accumulated charges on the spacer.

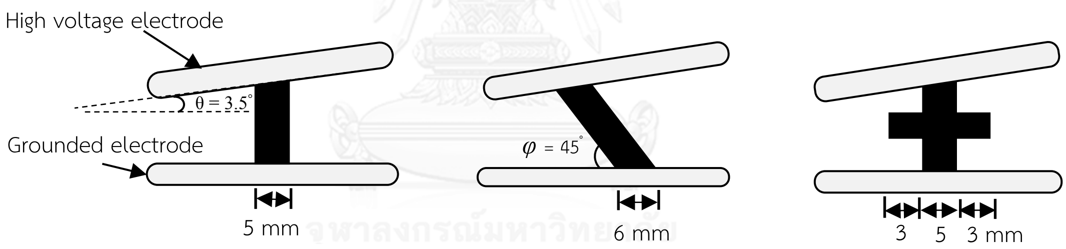

(a) Trapezoidal (b) Inclined (c) Cone and rib

Figure 1.2 Electrode arrangement for observing particle motion around spacers.

1.2.4 Calculations of corona inception voltage in air

Kubuki et. al. used the models and the experiment of sphere-sphere electrodes with a floating particle to estimate breakdown voltage in air. Both sphere electrodes had 62.5 mm diameters and the electrode separation was 40 to 400 mm [20]. The particle was stainless steel needle with hemispherical ends. The particle length was 20 mm. The criteria used to estimate breakdown voltage was

$$\int_0^{x_c} \overline{\alpha} dz = K \tag{1.1}$$

where $\bar{\alpha}$ is the ionization coefficient, x_c is critical avalanche length, and K is a constant value which is set to 10.

They found that the breakdown initiated from the particle. In the analysis, the positive breakdown voltage was almost constantly independent with position of the particle, but the negative breakdown voltage increased linearly with increasing gap between the particle and the grounded electrode. The difference of positive breakdown voltage between experimental and analytical values was largest where the particle in contact with high voltage electrode, and with the grounded electrode for the negative breakdown voltage.

Hiziroglu et. al. studied and analyzed the breakdown voltage in short air gap [21]. For the first experiment, two sphere electrodes were placed vertically above the ground plane. The lower sphere was also grounded. For the second experiment, only one sphere was placed above the ground plane. Two spheres had diameters of 22 cm, and the grounded plane electrode had dimensions of 240 cm by 300 cm. The gap between electrodes was set from 2 to 10 cm. The streamer criteria was also calculated by equation (1.1). K was constant value which was set to 18.5. They calculated $\bar{\alpha}$ by

$$\frac{\bar{\alpha}}{p} = A_i + B_i\left(\frac{E}{p}\right) + C_i\left(\frac{E}{p}\right)^2 \quad \text{for} \quad a_i < \frac{E}{p} < b_i \quad . \qquad (1.2)$$

where the coefficients (A_i, B_i and C_i) and the ranges (a_i and b_i) are given in table 1.1. From the results, the calculated breakdown voltages agreed with measured ones with error 0.42–2.40 %.

Petcharaks investigated streamer breakdown criteria which were modified by many authors to match with their experimental values [22]. Meek and Raether proposed equations as

$$E = k\frac{\bar{\alpha}e^{\bar{\alpha}d}}{\sqrt{d/p}} \qquad (1.3)$$

$$e^{\bar{\alpha}d} = \psi d \qquad (1.4)$$

For equation (1.3), Meek, Sanders and Friedrich set k equal to 4.8×10^{-8}, 3.6×10^{-7} and 5.6×10^{-5}, respectively. Friedrich also suggested that K = 9.15 for equation (1.1) to compare with equation (1.3). For equation (1.4), Meek, Sanders and Friedrich set values of ψ equal to 3×10^{6}, 2.1×10^{6} and 1.5×10^{4}, respectively. The modified criteria of Friedrich and Sanders were compared with experimental data of spherical electrodes with 5–100 mm gap. The results showed that the criteria proposed by Sanders for dry air were not accurate in dry air. The value was too high for calculation of breakdown voltage. The criteria proposed by Friedrich was more accurate with $k=5.6\times10^{-8}$ and $\psi=1.5\times10^{4}$ in equations (1.3) and (1.4), respectively. The breakdown or inception voltages could be calculated with value of K = 9.15 in equation (1.1).

Table 1.1 Coefficients (A_i, B_i and C_i) and the ranges (a_i and b_i)

i	A_i	B_i	C_i	$a_i (V/cm\,torr)$	$b_i (V/cm\,torr)$
1	8.10×10^{-3}	-1.29×10^{-3}	3.28×10^{-5}	25	30
2	3.87×10^{-2}	-3.37×10^{-3}	6.80×10^{-5}	30	35
3	1.32×10^{-1}	-8.57×10^{-3}	1.40×10^{-4}	35	40
4	1.69×10^{-2}	-2.64×10^{-3}	6.40×10^{-5}	40	45
5	-3.98×10^{-1}	1.41×10^{-2}	-1.04×10^{-4}	45	50
6	6.49×10^{-1}	-2.80×10^{-2}	3.20×10^{-4}	50	55
7	5.28×10^{-1}	-2.14×10^{-2}	2.40×10^{-4}	55	60

1.3 Problem statement

Particle-initiated partial discharge is a complex phenomenon, which is influenced by many factors. The researches aims to clarify the corona discharge initiated by particles. The particles treated in the thesis are in various geometrical forms, having different ending profiles.

1.4 Objective and scope of work

The purpose of this research is to clarify the effect on the partial discharge from the following factors:

1. Tip profile: rounded, flat, sharp, very-sharp tip and spheroidal particles
2. Charging condition: charged and uncharged particles
3. Contact condition and separation from an electrode: particles standing in contact with or floating above the grounded electrode.

The research is limited to the study of corona inception and charge associated with corona under positive DC applied voltage because the negative corona discharge is easier to take place than the positive corona discharge. For separation condition, the particles are floated by small distances above the grounded electrode in comparison with the total gap length.

1.5 Thesis organization

The contents of thesis are organized as follows:

Chapter I presents introduction, objective, scope and literature reviews.

Chapter II presents Theory and theoretical background, fundamental of corona discharge and calculation of corona inception voltage.

Chapter III presents setup and procedure for the particles standing on and floating above the grounded electrodes.

Chapter IV presents results of standing and floating particles

Chapter V presents analysis results

Chapter VI presents conclusion.

CHAPTER II

FUNDATIONAL OF CORONA DISCHARGE

2.1 Corona discharge

Corona is originally from a French word “couronne”, which means crown. It usually takes place in a short period, but repeats in time. It can be detected by the blue or violate light of discharge current. Figure 2.1 shows an example of positive and negative discharges in a 40 mm point-plane electrode gap at 1 bar atmospheric air under DC applied voltages. The upper and lower dot lines are the position of point and plane electrodes, respectively. The discharge is initiated from the point electrode, and propagates to the plat electrode. The luminous filaments extend with higher applied voltage.

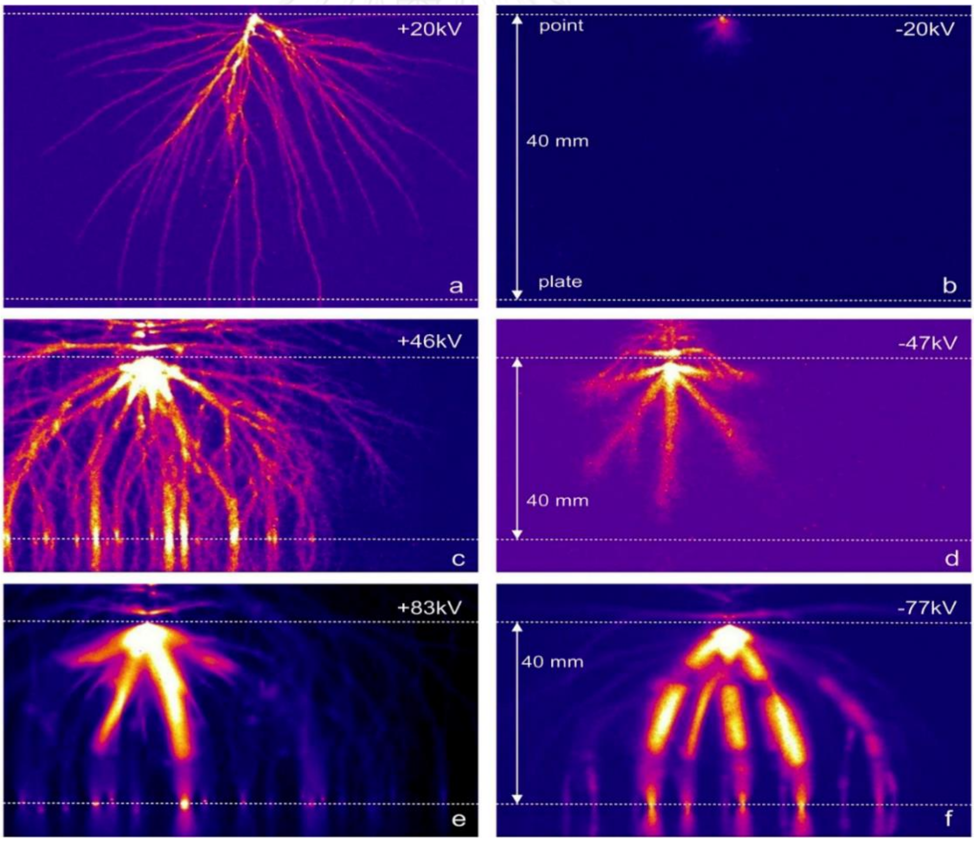

Figure 2.1 The positive (left column) and negative (right column) corona discharges in point-plane electrode under DC applied voltage. [23].

2.2 Influencing factors of **corona** discharge

The corona discharge has many forms depending on voltage sources, which are DC, AC, or combination of types. The corona discharge behavior is affected by many factors such as polarity of applied voltage, environment factors, electrode curvature radius or others.

2.2.1 Applied voltage

When a positive voltage is applied to a rod electrode until electric field is higher than critical value, electron avalanches move toward the rod electrode, and positive ions move away from the rod electrode due to opposite polarity of the rod electrode, as shown in Figure 2.2(a). Because of high mobility, the electrons move rapidly to the rod electrode and are neutralized. The positive ions form cloud, and move slowly to drift region [24]. The space charge of positive ions reduces the electric field at the rod electrode side and increases the electric field further away from it. The field distorted by positive space charged is shown in Figure 2.2(b). Therefore, the ionization process near the rod electrode is weakened, and the positive corona discharge is suppressed to take place at stronger field stress. [25]

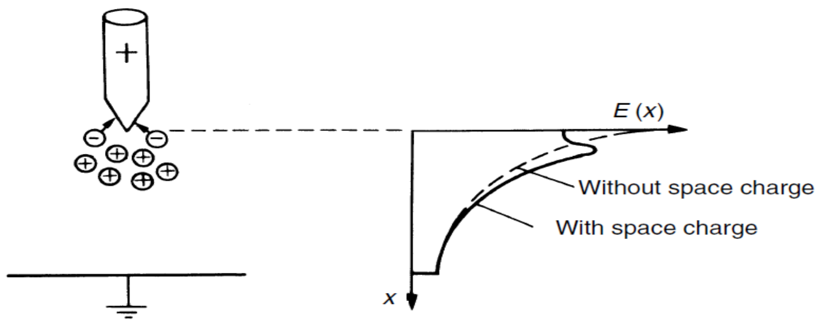

(a) Electron avalanche near rod electrode (b) Electric field distortion by space charge

Figure 2.2 Corona under positive applied voltage [25].

Positive corona discharge starts in a form of burst pulse, and processes to streamer corona, glow corona and spark when applied voltage increases [26]. Figure

2.3 shows the typical positive corona discharges. When the applied voltage is below the onset voltage of burst pulse, there is no self-sustainment of discharge between electrode gaps. A little increase of voltage above voltage of burst pulses, a large number of electrons generated from electron multiplication process appears and the discharge spreads over the rod electrode. The small branches with light phenomena are initiated from the rod tip of electrode under positive applied voltage in short time, called burst pulse, shown in Figure 2.3(a). The preceding pulses have shorter and weaker light. When the voltage increases, the efficiency of ionization process increases, and the current density near rod electrode vicinity rises. Therefore, the burst pulses develop with longer length and larger number of branches, called streamer, shown in Figure 2.3(b). The branches of streamer never cross to each other. The velocity of the streamer increases in the high electric region, but decreases in low electric field region. The Figure 2.4 shows the propagation velocity of axial streamer in 2.5 cm air gap [25]. When the voltage is applied to rod electrode with 1-cm radius tip for long time, the ionization process has sufficient time to wander the gap and accumulates in space. That results electric field distortion. The streamer head has positive charge density approximately 10^{8} –10^{20}/m^{3} with diameter from 20 to 200 μm [27]. When the streamer disappears, the discharge gap is filled with the space charge of positive ions. The new generation of streamer re-appears when the space charge is removed far enough from the rod electrode and the field strength recovers.

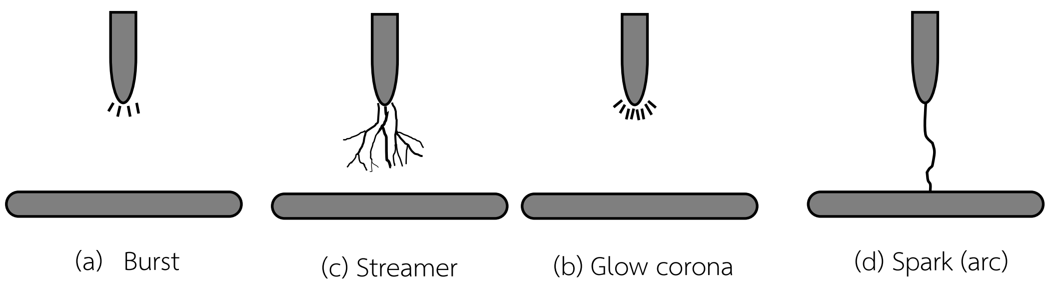

Figure 2.3 Typical positive corona discharges in rod-plane electrode.

When the applied voltage keeps increasing further, the repetition rate of streamer increases, and the streamer becomes self-sustainment. Then, it develops to steady glow at the rod electrode with fluctuate current. The glow corona is shown in

Figure 2.3(c). When the applied voltage increases still further, the new and more vigorous glows develop to complete breakdown as shown in Figure 2.3(d). A strong luminous filament appears in the whole gap of electrodes.

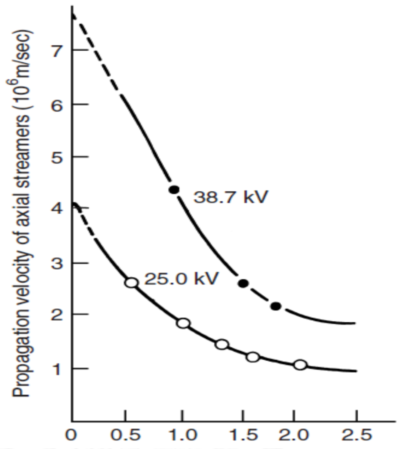

Figure 2.4 propagation velocity of axial streamer in 2.5 cm air gap [25].

When a negative voltage is applied to the rod electrode, the electrons move rapidly to the low field region. They attach gas molecules and tend to hold back the positive space charge which remains in the space between the negative charge and the rod electrode. The positive ions move slowly to the rod. Because of low mobility, the positive ions concentrate in form of cloud near the rod electrode. These ions distort electric field, increasing electric field near the electrode, but reducing the ionization region.

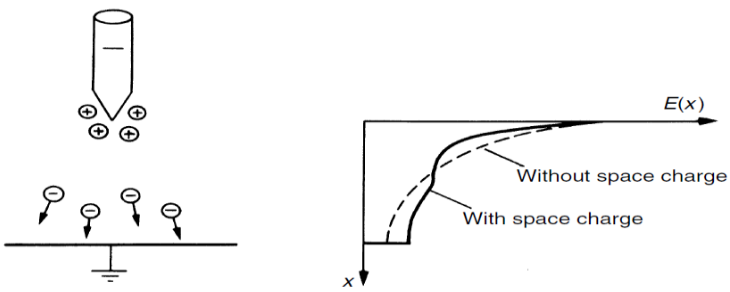

(a) Positive ions cloud near rod electrode (b) Field distortion by space charge

Figure 2.5 Negative corona discharge in the rod-plane electrode [25].

When negative DC applied voltage increases until the first observable pulses appear, they are called Trichel pulses. The pulses lead to glow and spark as shown in Figure 2.6. The repetition rate of Trichel pulses, shown in Figure 2.6(a), increases with increasing voltage. When the pressure decreases, the repetition rate of pulses decreases. A little increasing of applied voltage, the pulses join in a continuous plateau. The luminous pulses decrease and accumulate others at the space region, called glow corona as shown in Figure 2.6(b). Figure 2.7 shows the corona development under negative applied voltage in the air gap between the rod and plane electrodes. The gap length slightly affects Tichel onset voltage. The steady glow discharge still persists with raising wide range of onset voltage. When the applied voltage increases above the glow corona level, the glow discharge transitions to spark, shown in Figure 2.6(c).

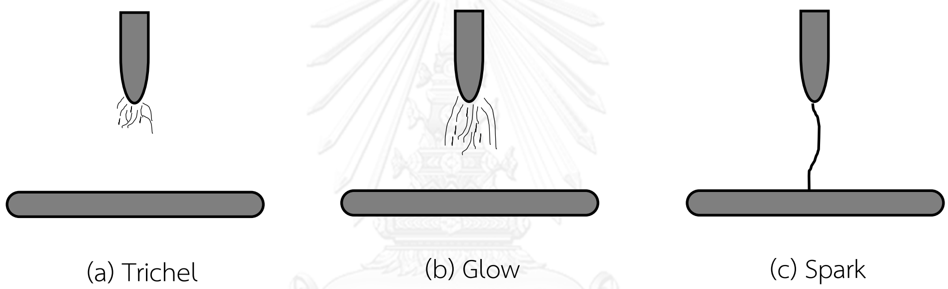

Figure 2.6 Typical negative corona discharges in rod-plane electrode.

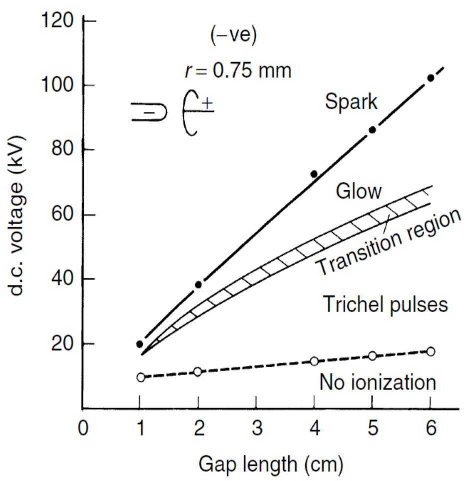

Figure 2.7 Development corona discharge in 0.75 radius rod-plane electrode from Trichel pulse to glow and Spark [25].

2.2.2 Environmental factors

Corona discharge has relationships with environment factors such as gas pressure, humidity and temperature. When the gas pressure is low with increasing applied voltage, the luminous of discharge current becomes brighter [28]. The luminary becomes brighter as the current increases. When the pressure increases, the luminary becomes smaller and disappears.

The humidity is considered to affect current and voltage characteristic [29]. In the experiment in wire-plane electrodes under positive or negative applied voltages, the corona current and voltage decrease significantly with increasing humidity because present of water vapor in air increases the attachment coefficient of mixture (air and water) and the ionization coefficient is constant. In addition, the mobility of ion decreased with increasing humidity.

Base on the experiment carried out in temperature range between 20–40° C, the temperature affects PD characteristic in needle-bowl electrode configuration under AC applied voltage with low frequency (0.1–50 Hz) [30]. The electrode system is placed in an enclosed chamber. The PD charge magnitude and voltage do not change significantly when the temperature is between 20–30°C. When the temperature increases from 30–40°C, PD inception voltage decreases, and the PD charge magnitude increases.

2.3 Physical process of ionization

Under a normal condition, gas is an excellent insulation. High electric field excites an electron to gain energy to ionize with an atom or molecule on the mean free path in direction of the field [31]. That is called direct ionization, which can be shown as

$$e^- + AB \rightarrow AB^+ + 2e^- \tag{2.1}$$

where e^- is an electron. AB and AB^+ are molecule, and positive ion after collision with the electron. After the direct ionization, an extra electron is liberated, but it does not have enough energy for ionizing. It transfers certain amount of kinetic energy to another molecule it collides with.

$$AB + e^{-} + KE \rightarrow AB^{*} + e^{-} \tag{2.2}$$

Where AB^{*} molecule receives energy transferred from the electron, KE is kinetic energy.

If the energy is smaller than that of the ionizing energy, it is absorbed by another molecule. If the energy exceeds the ionizing energy, the molecule with the energy generates one or more electrons.

For an experiment on the discharge current in two parallel plate electrodes at atmospheric air, the discharge current grown in gas is a function of applied voltage [24]. Figure 2.8 shows the process of current grown with applies voltage. The current increases proportionally with applied voltage V_1 when the applied voltage reaches onset corona voltage. At one voltage level, the current i_0 keeps constant at saturation point although the applied voltage increases further. When applied voltage increases from V_2 to define level. The current increases by an exponential rate.

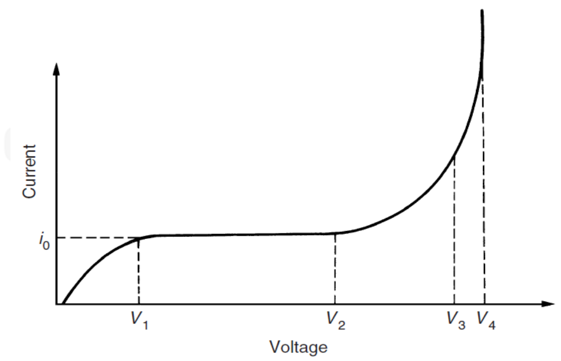

Figure 2.8 Curve of grown current with applied voltage [25].

Townsend's first ionization α expresses the increasing current in exponential rate leading to partial discharge [27]. Let n_0 be the number of initial electrons generated from distance (x = 0) from the cathode in electric field's direction. They will drift under the influence of electric field $E(x)$ with velocity $V = \mu_e E(x)$ where μ_e is the mobility of an electrons. If η is attachment coefficients, the increased electrons number dn along the drift length dx is

$$dn = (\alpha - \eta)n(x)dx = \overline{\alpha}n(x)dx \tag{2.3}$$

By integrating both side of equation (2.3), we have

$$n = n_0 \exp(\int_0^x \overline{\alpha} dx) \tag{2.4}$$

The exponential term in equation (2.4) is called electron multiplication. In case of the discharge in nonuniform electric field, the number of electrons reaches about 10^3–10^8. The region between electrodes is divided into ionization (α > 0) and drift regions (α < 0).

CHAPTER III
EXPERIMENT

3.1. Experimental setup

Experiments are set up to investigate the characteristic of partial discharge (PD). We use two configurations of particles in the experiments. For the first configuration, the particles are set to stand in contact with the grounded (lower) electrode. For the second configuration, the particles are hung above the grounded electrode by various gaps.

3.1.1 High voltage supplies

Two DC high voltage supplies are used in separated experiments. For the experiment on standing-particle configuration, a high voltage test transformer, a 2-stage Cockcroft-Walton rectifier circuit, a 13.9-MΩ limiting current resistor, and a control panel are used, as shown in Figure 3.1. The circuit has voltage rating of 200 kV. The test transformer rating is 220 V/ 100 kV and 5 kVA. The control panel is connected to a variac to change the primary voltage of the test transformer. The output voltage of the test transformer is converted to DC voltage by using the rectifier, which is connected in series to the current limiting resistor and the electrode system. The circuit diagram is shown in Figure 3.2. For the experiment on floating-particle configuration, a solid state 20 kV, 2.2 kW HV power supply (Matsusada, Model AU SERIES 2.2 kW), shown in Figure 3.3, is used.

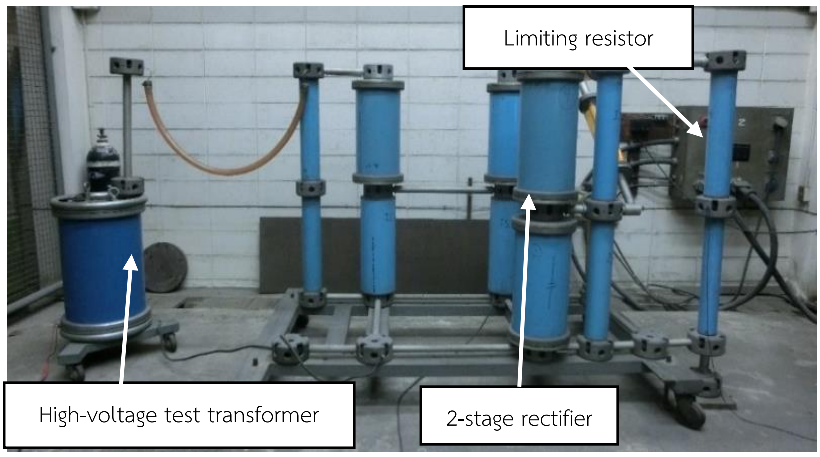

Figure 3.1 High voltage supply by a rectifier circuit for the standing particle-configuration.

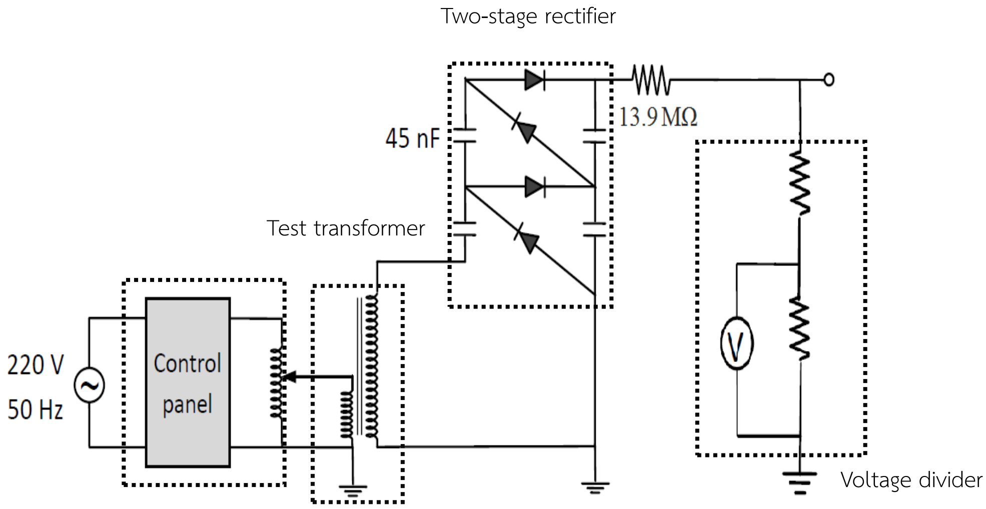

Figure 3.2 Schematic circuit diagram of applied voltage for the experiments of standing-particle configuration.

Figure 3.3 Solid state HV Power Supply for the experiments of floating-particle configuration.

3.1.2 Electrode system

Figure 3.4 shows the electrode system used in the experiments. The upper electrode has a diameter of 94 mm, and height of 20 mm. The electrode shape follows the Rogowski's profile approximately to avoid breakdown at the edge of electrode. The grounded electrode has a diameter of 140 mm and a solid cylinder (20 mm diameter) at its center. An insulating film is used to separate the grounded electrode from the solid cylinder to avoid PD current flowing directly to ground through the grounded electrode. The solid cylinder is connected to the ground through R_m, which is equal to 50 and 500 Ω to ground. PD current waveforms measured from R_m = 50 Ω is expected to minimize the wave distortion. By using R_m = 500 Ω, PD current can be detected at smaller magnitude. The voltage across R_m is measured by a 2 GS/s oscilloscope (Tektronix, TBS1202B-EDU) connected with a 50 Ω double-shielded cable to detect the PD current waveforms. The input impedance of oscilloscope is 1 MΩ and 20 pF. The waveforms are saved in a USB storage, and transferred to a personal computer.

3.1.3 Particles

Different kinds of particles are used for the experiments on standing or floating particles. Three samples are used for each kind of particles. All of them have 1-mm diameter and 4-mm length. They are made by aluminum. Their shapes are spheroidal or wire. The wire particles are prepared from aluminum (AL-011487 Nilaco).

The experiments of standing particles use three kinds of wire particles and the spheroidal particle. The wire particles have flat lower tips and the upper-tip shapes are rounded, sharp, or very sharp. The images of the standing particles are shown in Figure 3.5.

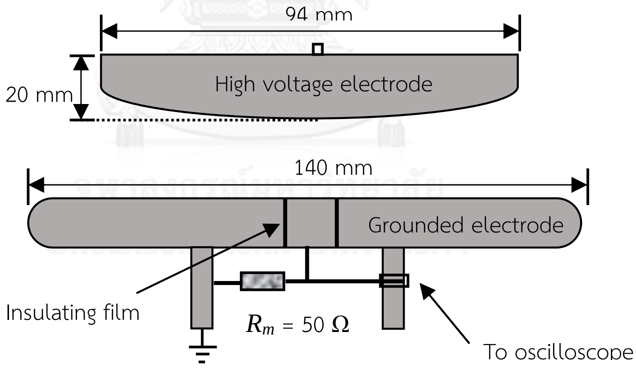

(a) Illustration of electrode system

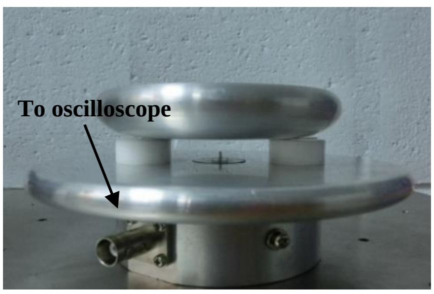

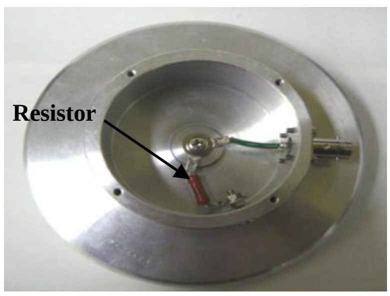

(b) Image of electrode (c) Bottom view of grounded electrode

Figure 3.4 Parallel electrode system used for standing or floating-particle configurations.

The experiments of floating particles also use four kinds of particles. For this configuration, the lower-tip shapes are also varied as they affect the electric field between the particles and the grounded electrode. The particles are identified as F-F, F-S, S-F, or S-S. The A-B notification specifies the particle upper and lower tips. For example, an F-S particle has a flat upper tip and a sharp lower tip. The images of the floating particles are shown in Figure 3.6.

(a) Rounded-tip (b) Sharp-tip (c) very-sharp tip (d) Spheroid

Figure 3.5 Images of the particles for the experiments in the standing configuration.

(a) Flat-Flat (F-F) (b) Flat-Sharp (F-S) (c) Sharp-Flat (S-F) (d) Sharp-Sharp (S-S)

Figure 3.6 Images of particles for the experiments in the floating configuration.

3.2 Procedure

3.2.1 Standing-particle configuration

The particles are set to stand perpendicular to the solid cylinder by using a rounded silicon plate (1 mm thickness) as shown in Figure 3.7. The flat tips of particles are in contact with the solid cylinder. The grounded electrode is separated from the upper electrode by 10 mm high spacers, while positive DC high voltage is applied to the upper electrode. The voltage is increased with a step of 0.06 kV approximately until PD current is detected by the oscilloscope. The high voltage is measured by using resistive voltage divider, which is connected in parallel with the electrode system. The experiments are repeated 10 times for each samples of the particles.

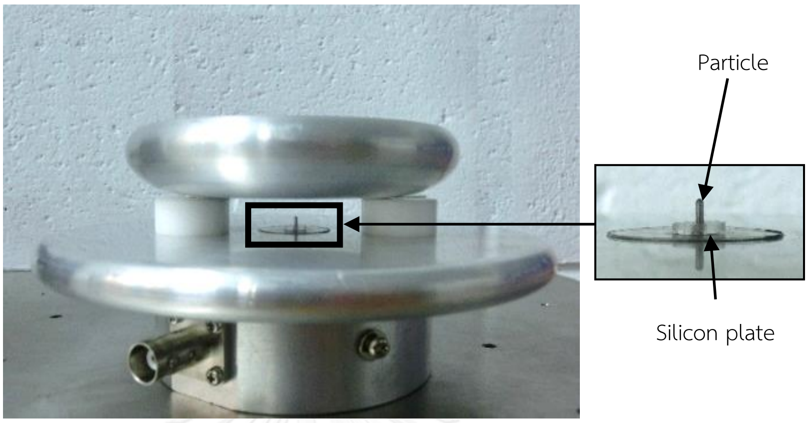

Figure 3.7 Standing-particle configuration.

3.2.2 Floating-particle configuration

A hole of 0.5 mm is drilled on the wire particles. A nylon wire with diameter of 0.4 mm is inserted through the hole, and the two ends of the nylon wire are attached to two acrylic poles by rubber bands. The upper electrode is fixed with a bakelite plate which is connected to z-axis moving stage. The grounded electrode is also supported by z-axis moving stage to vary the gap. The upper electrode is separated by 12 mm from the grounded electrode. The details of electrode system are shown in Figure 3.8.

For the experiments on floating particles, Ethanol is sprayed on the particles to eliminate the charge in the particles for every experimental runs. The particles are hung by 0.25, 0.5, 1, 1.5 or 2 mm above the grounded electrode. Then, the positive voltage applied to the upper electrode is increased by rating of 0.1 kV/s approximately until the first PD current is detected. The waveforms are recorded. The experiments are repeated 10 times for each samples of the particles.

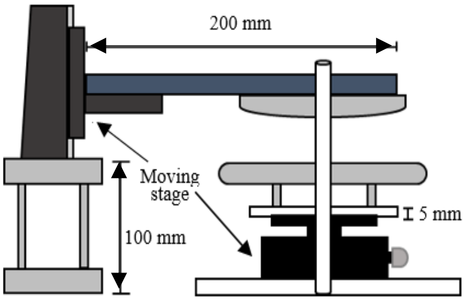

(a) Illustration of side view

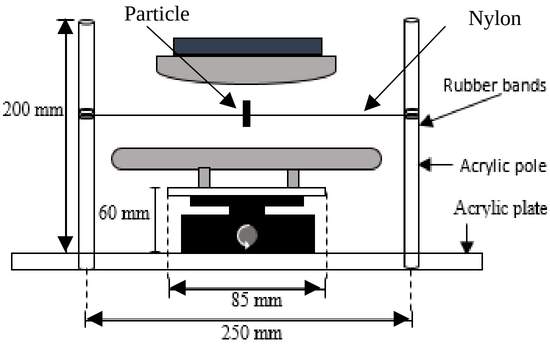

(b) Illustration of front view

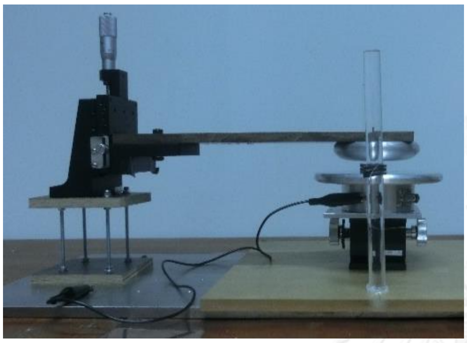

(c) Actual side view

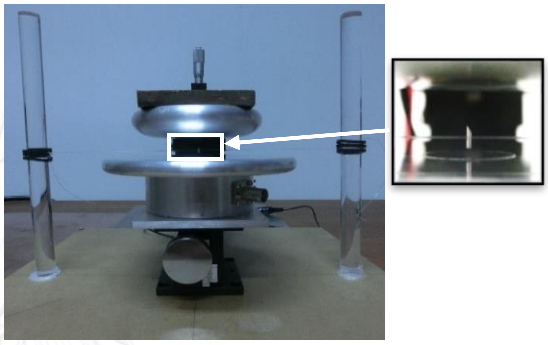

(d) Actual front view

Figure 3.8 Illustrations and Images of floating-particle configuration.

CHAPTER IV
EXPERIMENTAL RESULTS

4.1 Standing-particle configuration

4.1.1 PD inception voltage

When a positive voltage is applied to the upper electrode, ionization takes place at the particle tip. The electrons move toward the upper electrode, while positive ions accumulate near the particle tip. The inception corona takes place at the particle tip, where the electric field is the highest. Figure 4.1 shows the average values of corona inception voltage U_i measured from two values of R_m, 50 Ω or 500 Ω. The average values of U_i were taken from 30 experimental runs. The error bars present the maximal and minimal U_i values from the experimental runs. From the figure, the measured U_i in the case using 50 Ω R_m did not differ significantly from those using 500 Ω. For the wire particles, the rounded-tip particle had the highest measured U_i and the very-sharp tip particle had the lowest measured U_i. The measured U_i of the spheroidal particle was between those of the rounded and sharp tip particles.

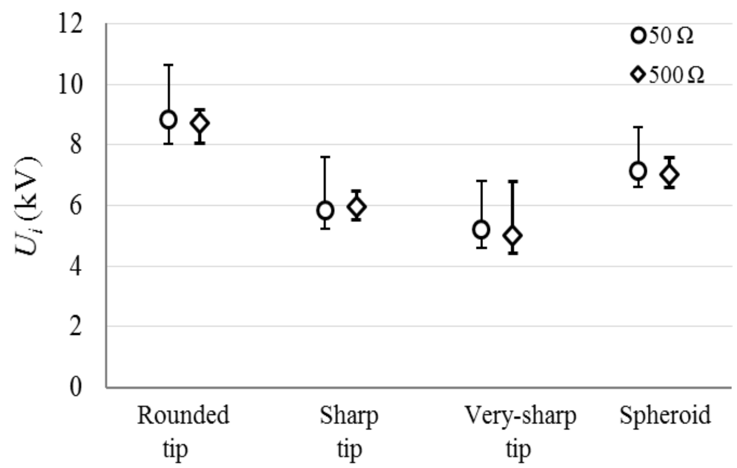

Figure 4.1 PD inception voltage measured from R_m = 50 and 500 Ω for the standing particles.

4.1.2 PD current waveforms

Figure 4.2 shows an example of the waveforms of the PD currents measured from 50 **Ω** R_m for the standing particles. The rise time of PD current pulse (limited by response of oscilloscope and the measuring circuit) was about a few ns to reach the peak. PD current magnitudes followed the tendency of the measured U_i values in Figure 4.1 as they were higher when the U_i values were higher. The duration of discharge was about 0.25 μs. The oscillation of the waveform was caused by the input impedance of oscilloscope. The effect of the input impedance of the oscilloscope on the measured PD current waveforms is shown in Appendix.

Figure 4.3 shows an example of PD current waveforms measured from R_m = 500 **Ω** for the standing particles. The tendency of current waveform magnitudes also followed the tendency of the measured U_i in Figure 4.1. The rise time for the case using R_m = 500 **Ω** was longer than that for the case using R_m = 50 **Ω**. The current magnitudes for case 500 **Ω** were lower than the case using R_m = 50 **Ω** for all particles.

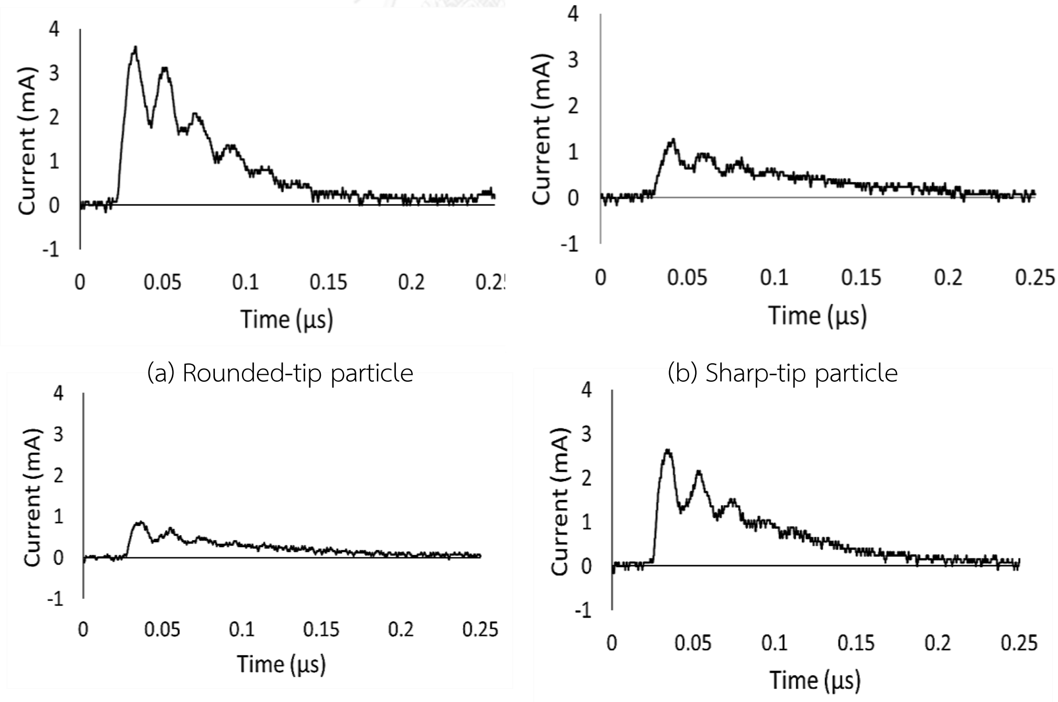

(a) Rounded-tip particle

(b) Sharp-tip particle

(c) Very-sharp tip particle

(d) Spheroidal particle

Figure 4.2 PD current waveforms measured from R_m = 50 **Ω** for the standing particles.

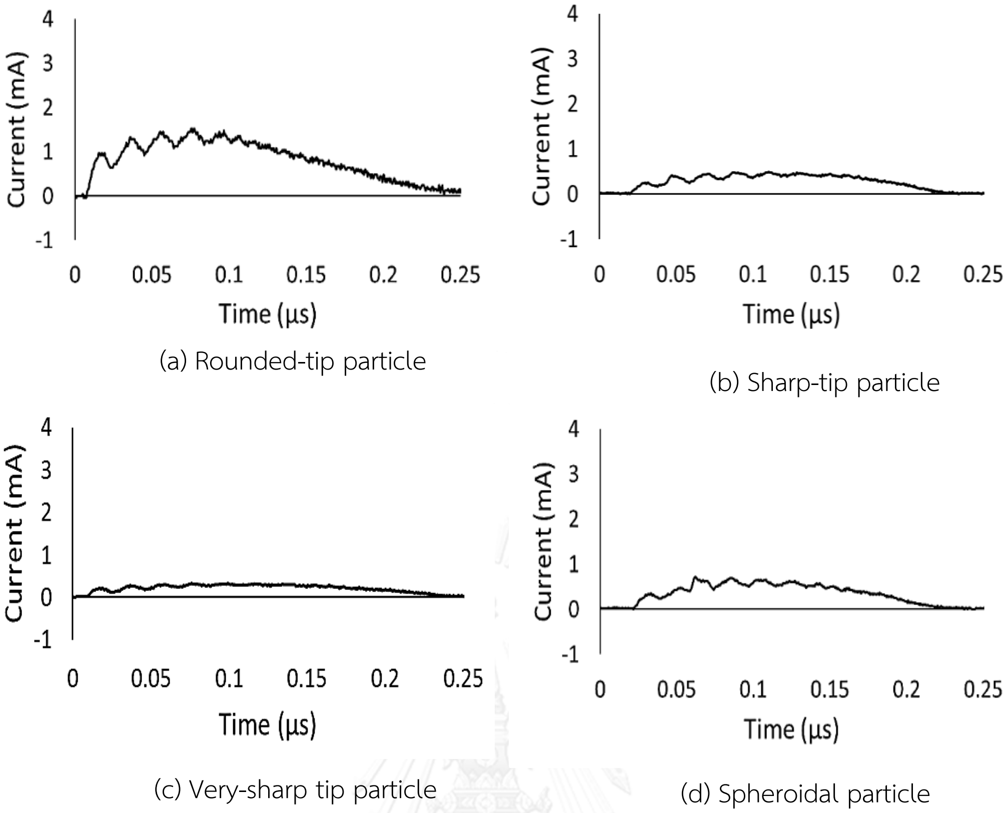

(a) Rounded-tip particle

(b) Sharp-tip particle

(c) Very-sharp tip particle

(d) Spheroidal particle

Figure 4.3 PD current waveforms measured from R_m = 500 Ω for the standing particles.

4.1.3 PD charge

Figure 4.4 presents the average PD charge Q_{PD} measured from R_m = 50 and 500 Ω, associated with partial discharge on the particle at the PD inception voltage for the standing particles. Q_{PD} was obtained by integrating current waveform for an interval of 0.25 μs for 50 Ω and 1 μs for 500 Ω because the duration of some discharges in the case using 500 Ω was longer than 0.25 μs. The error bars in the figure represent the maximal and minimal Q_{PD}. The average Q_{PD} values in the case R_m = 50 and 500 Ω were not much different even the variation of Q_{PD} were large from each experimental runs. The rounded-tip particle had the highest average Q_{PD} and lowest for the very-sharp tip particle. The average Q_{PD} of the spheroidal particle was between Q_{PD} of the rounded and sharp-tip particles. The tendency of average Q_{PD} was the same as the measured U_i in Figure 4.1.

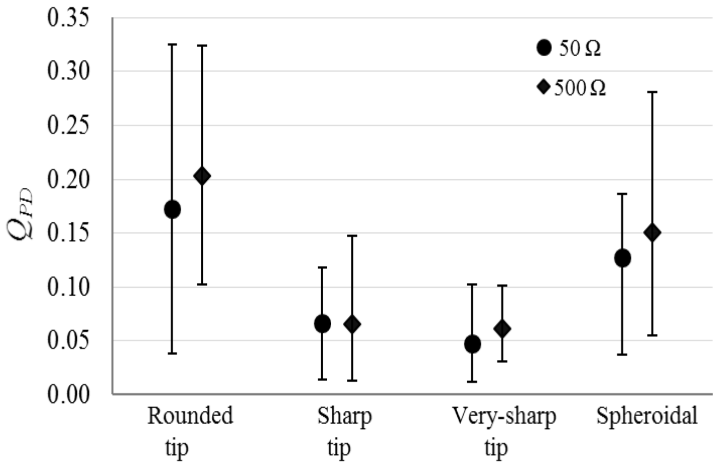

Figure 4.4 PD charge measured from R_m = 50 and 500 Ω for the standing particles.

4.2 Floating-particle configuration

4.2.1 PD inception voltage

When the particle is floated in electrode system, the particle is polarized under the external field. The positive and negative charges are induced on the tip facing the cathode and the anode, respectively. The discharge inception voltage was measured by using R_m = 50 Ω for floating particles. Figure 4.5 shows the measured results as a function of the gap g. The void plots present the PD inception voltage U_i, and the solid plots present the spark discharge voltage U_s (without preceding PD inception voltage). The particles with the flat upper tip (F-S and F-S) exhibited direct spark discharge U_s at smaller g values as shown in Figure 4.5(a) and (b). The spark occurred at longer ranges of g (0.25–1 mm) for the F-F particle than for the F-S particle. U_s of the F-F and F-S particle increased with increasing g. The tendency of U_i occurring at at longer gap g was not clear for the F-F and F-S particles. The particles with upper sharp tip (S-F and S-S) exhibited U_i for all gap lengths between 0.25–2.0 mm. U_i of the S-F and S-S particle increased with increasing g from 0.25–1.0 mm but decreased with increasing g for larger gap.

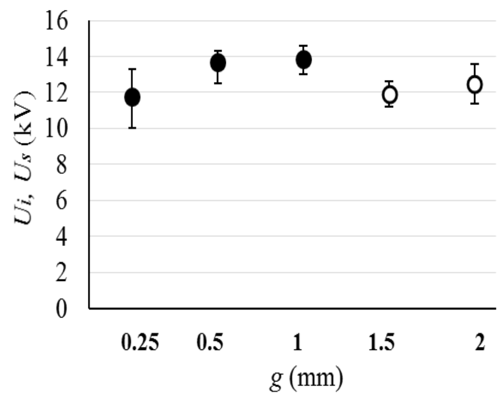

(a) Flat-Flat particle (F-F)

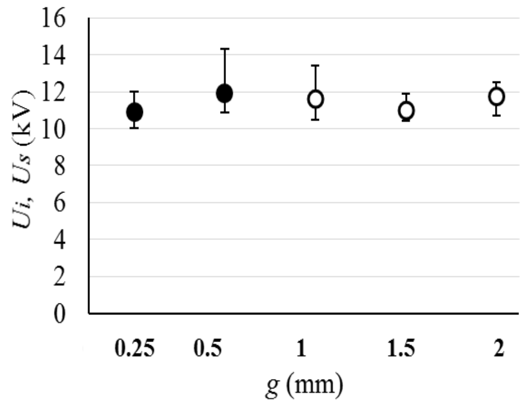

(b) Flat-Sharp particle (F-S)

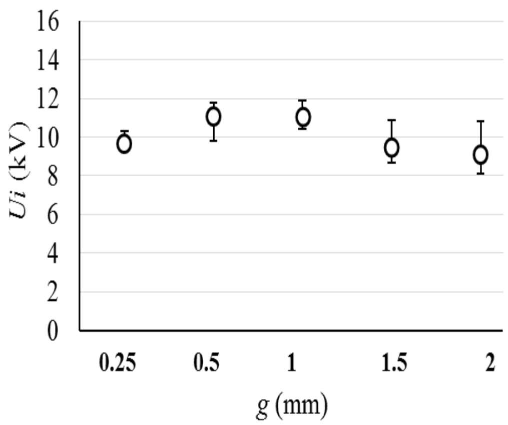

(c) Sharp-Flat particle (S-F)

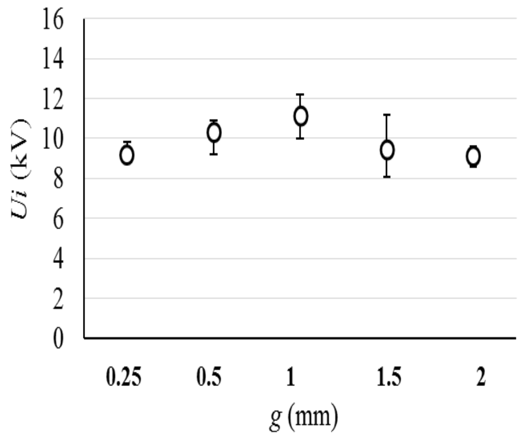

(d) Sharp-Sharp particle (S-S)

Figure 4.5 Discharge inception voltages as a function of gap length for the floating particles.

Figure 4.6 compares the average values of discharge inception voltage between the particles at each gap distance. At small gap (g = 0.25 or 0.5 mm), U_s was higher for the F-F particle than for the F-S particle. U_i was higher for the S-F particle than for the S-S particle. Therefore, the lower tip contributed to U_s and U_i for small gap lengths. At large gap (g = 1.5 to 2 mm), U_i of the F-F and F-S particle still showed the same contribution of the lower tip. The shape lower tip exhibited lower U_i values. On the other hand, the tendency of U_i for the S-F and S-S was not clear enough for conclusion. The F-F and F-S particles with flat upper tip exhibited higher U_i than the S-F and S-S particles.

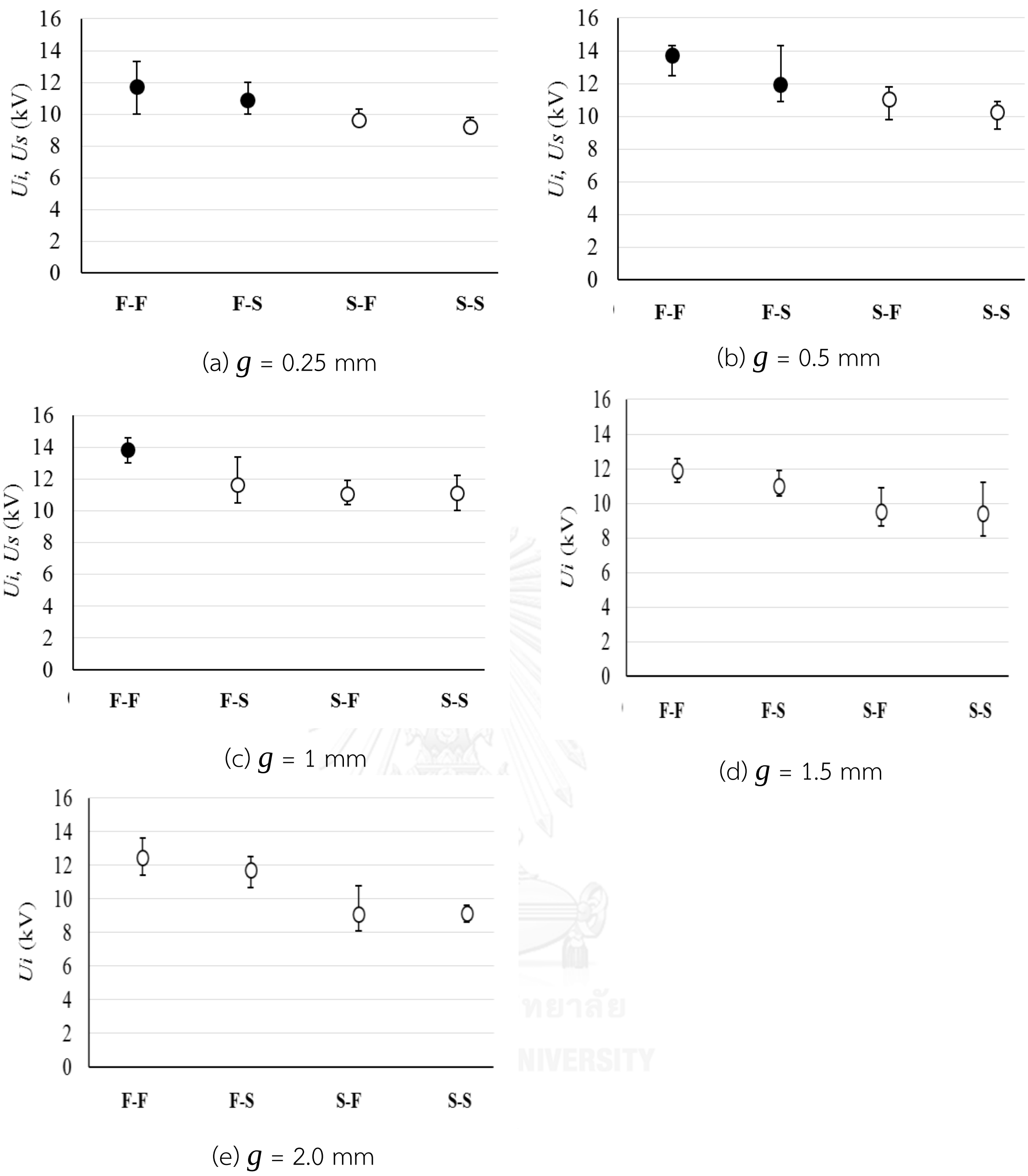

Figure 4.6 Discharge inception voltages as a function of tip profile for the floating particles.

4.2.2 Comparison of U_i with existing works

U_i of the F-F particle is used to compare with that of wire particle with two hemispherical tips. The hemispherical tip particle has length of 6mm and diameter of of 0.25 mm. The gap between the upper and lower electrodes was 20 mm. Figure 4.7 shows the discharge voltage as a function of gap lengths for the F-F particle and hemispherical tip particle. For Figure 4.7 (a), the F-F particle yielded spark discharge at small gap. In contrast, Figure 4.7(b) shows that the corona took place for all gap lengths because the hemispherical-tip particle has smaller diameter than the F-F particle by 4 times. Anyhow, the tendency of discharge inception voltage of both particles increased with increasing gap from 0 to 1 mm.

Figure 4.8 shows the corona onset voltage of the particle with two flat tips (the same shape as the F-F particles) from [14]. The results shows the corona onset was almost constant with increasing gaps. The tendency is different from that in Figure 4.7(a) because large increasing gap length (2 mm). The electric field is higher when the particle is closer to the grounded electrode, and it hardly varies with distance from the electrodes. Therefore, the corona onset is almost constant with increasing gap length.

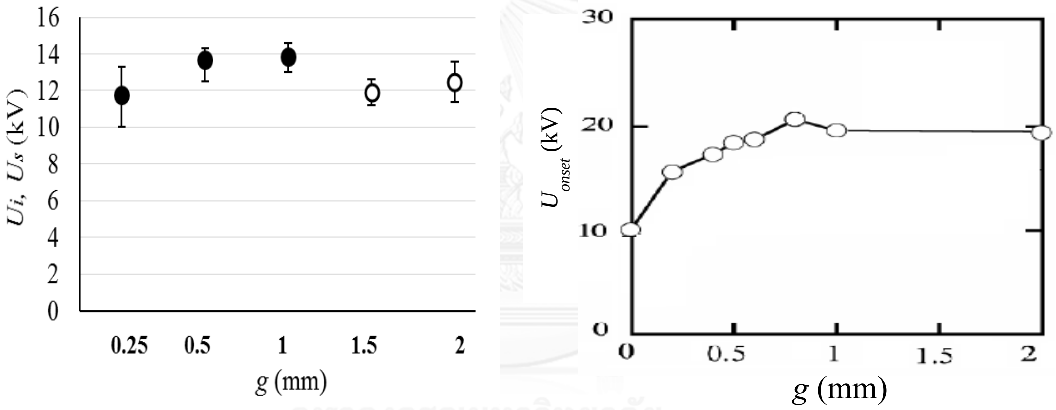

(a) F-F particle

(b) Hemispherical tip particle. Modified from [13]

Figure 4.7 Comparison of discharge inception voltage of particle with flat or hemispherical tips

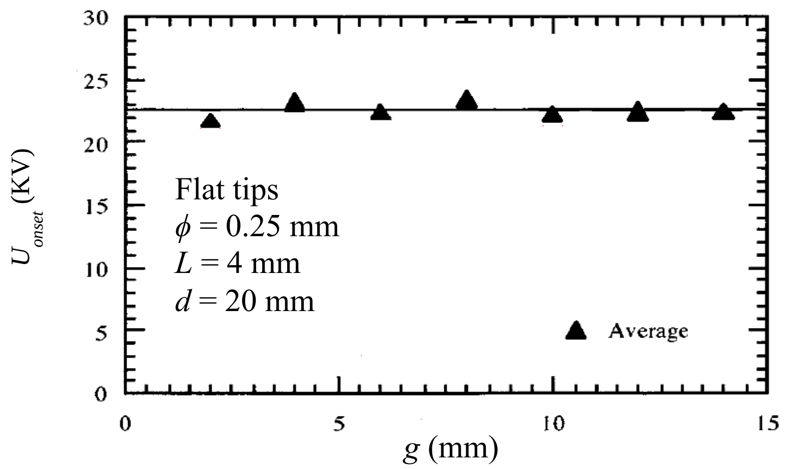

Figure 4.8 Corona onset voltage of particle with two flat tips.

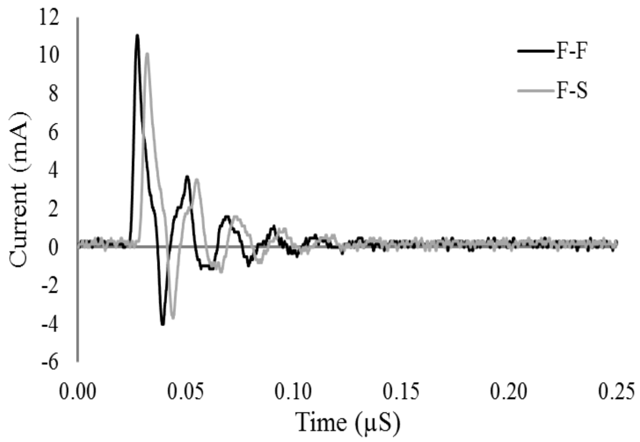

Figure 4.9 Spark current waveform of the F-F and F-S particles in the case g = 0.25 mm.

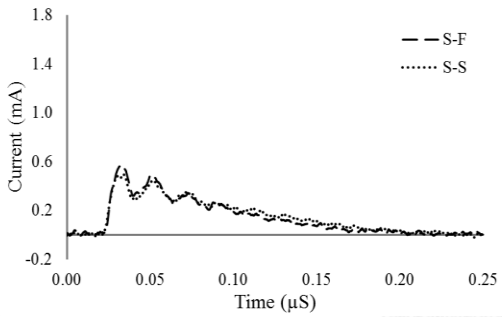

(a) g = 0.25 mm

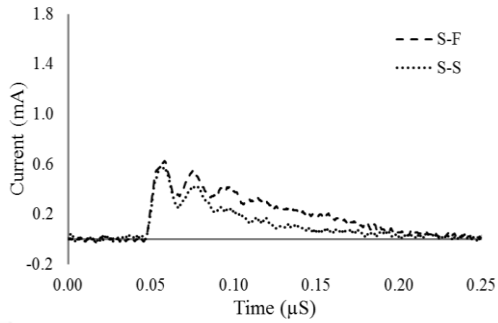

(b) g = 0.5 mm

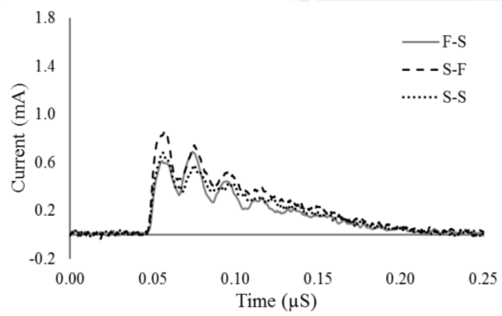

(c) g = 1.0 mm

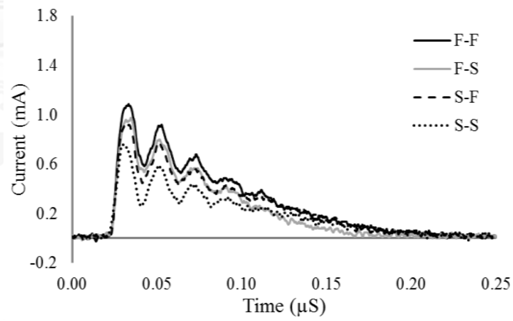

(d) g = 1.5 mm

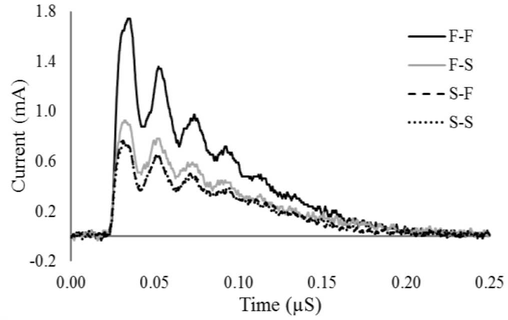

(e) g = 2.0 mm

Figure 4.10 PD current waveforms associated with the measured U_i for the floating particles.

4.2.3 PD current waveform

Figure 4.9 shows the discharge current waveforms obtained from the F-F and F-S particle in the case g = 0.25 mm. The discharge currents were from spark events. The current magnitudes were large and the reversion of current direction took place. When the spark took place, the total positive ions in the particle were transferred to ground, and the particle are negatively changed. Then, the positive charge flew for balancing of particle. Therefore, the current reversed from positive to negative values. For other cases of spark in Figures 4.5 (a) and 4.5(b), the waveforms were similar to the spark in the case g = 0.25 mm in Figure 4.9.

Figure 4.10 show of PD current waveforms of the floating particles. The rise times were a few nanoseconds. The PD current magnitudes in the case of the floating particles are lower than those in the case of the standing particles. Note that the current magnitudes of PD did not follow the tendency of U_i in Figure 4.6.

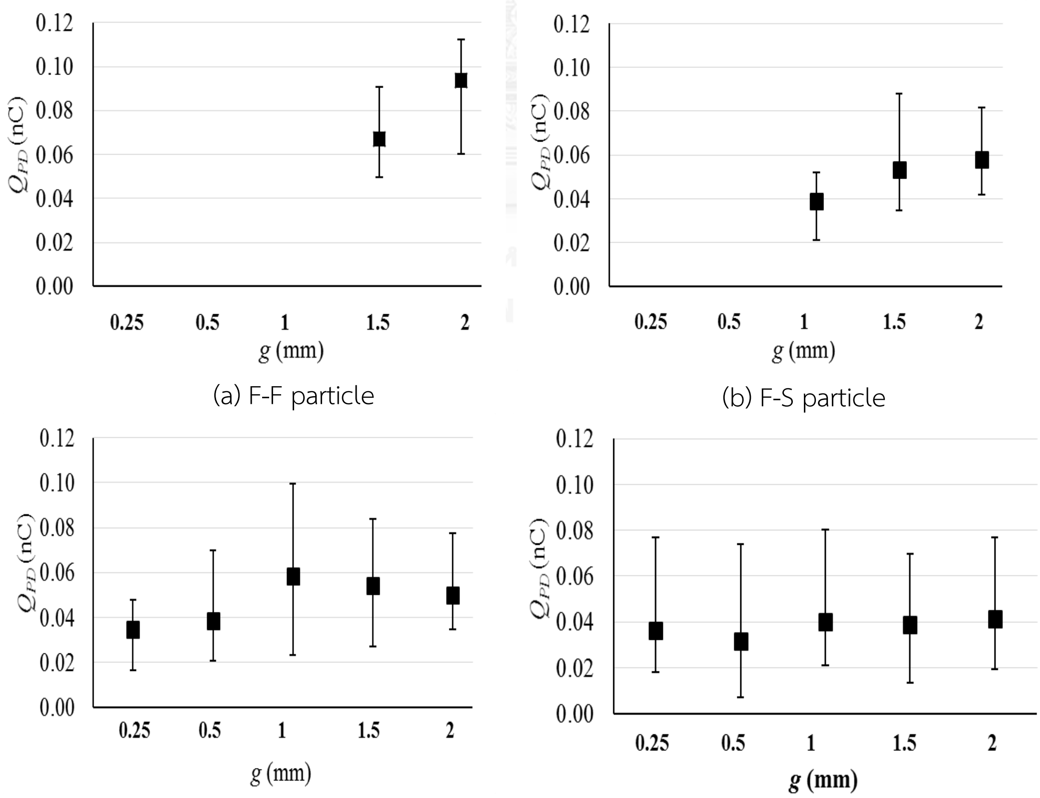

(a) F-F particle

(b) F-S particle

(c) S-F particle

(d) S-S particle

Figure 4.11 PD charge obtained from R_m = 50 Ω as a function of gap lengths for the floating particles.

4.2.3 PD charge

Figure 4.11 presents Q_{PD} associated with the measured U_i. Q_{PD} was obtained by integrating current waveform in Figure 4.10 for an interval of 0.25 μs. For g = 1.5 or 2 mm, Q_{PD} of the F-F and F-S particle was larger with increasing g. The Q_{PD} intended to follow the tendency of U_i in Figure 4.5. The relation of Q_{PD} and U_i of the F-F particles was not clear. Figure 4.12 shows Q_{PD} as a function of the particle profiles. Q_{PD} of the F-F and F-S particle followed the tendency of U_i in Figure 4.6. For smaller g (0.25–1 mm), the Q_{PD} of the F-F particle was largest and lowest for the S-S particles for all gap lengths.

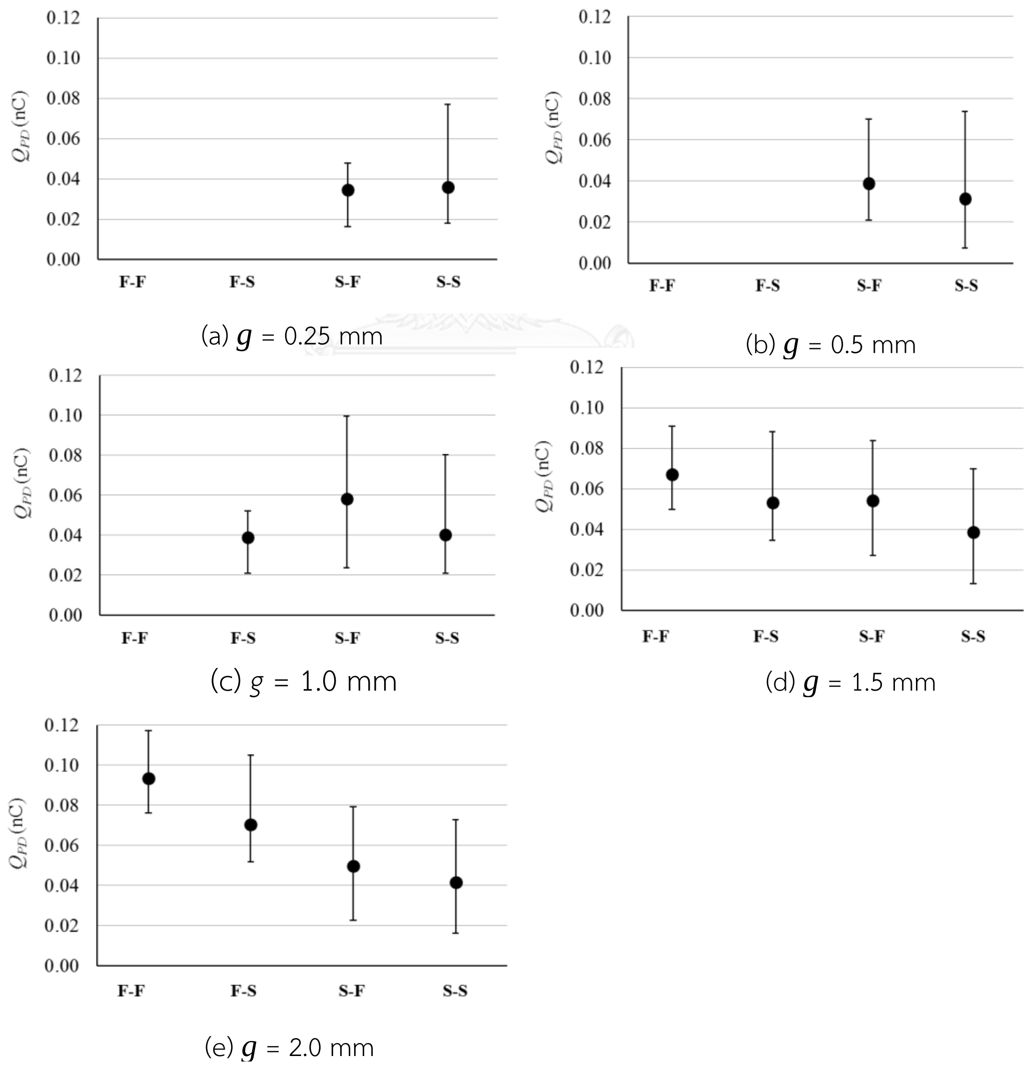

(a) g = 0.25 mm

(b) g = 0.5 mm

(c) g = 1.0 mm

(d) g = 1.5 mm

(e) g = 2.0 mm

Figure 4.12 PD charge as a function of particle profiles for the floating particles.

CHAPTER V
DISCUSSION

This chapter presents the analysis of the electric field, corona inception voltage, and particle charge for the standing or floating-particle configurations in relation to the experiments describing in chapter 4. The criteria based on breakdown streamer is used to calculate corona inception voltage.

5.1. Calculation of corona inception voltage.

5.1.1 Model

The Elmer software based on the finite element analysis is employed to simulate the electric field. The GiD software is used for the pre-processing (geometrical modeling). Figure 5.1 shows the axisymmetric models of standing or floating-particle configurations. A unit potential is applied to the upper electrode, and the lower electrode is grounded. Note that the models are simplified to be axisymmetric in order to reduce the calculation time and memory usage. Figure 5.2 shows the particle contours used for the standing and floating configurations. The sharp and very-sharp tips of the particles are approximated to have 0.02 mm radius, as shown in Figure 5.3.

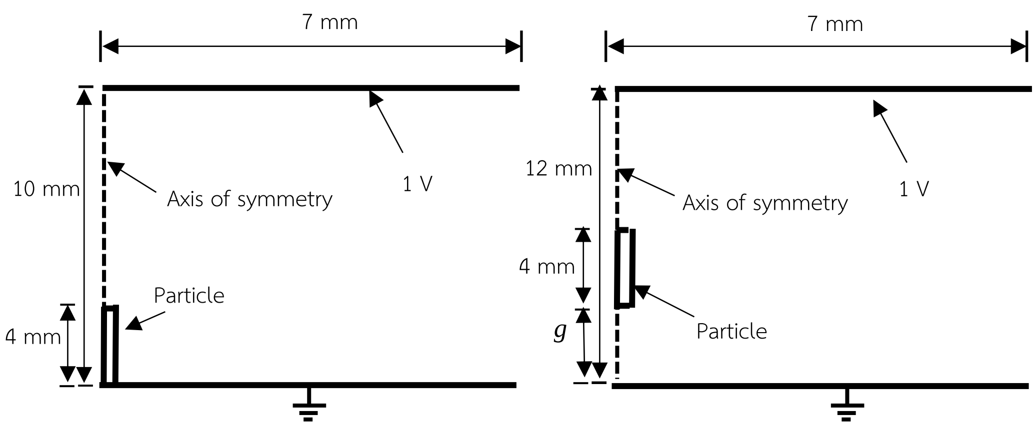

(a) Standing particle-

(b) Floating-particle configuration

Figure 5.1 Axisymmetric models.

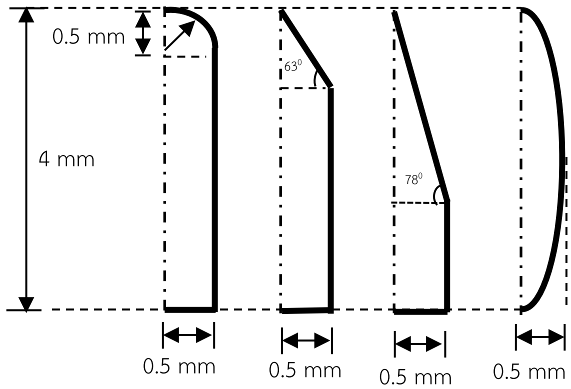

(a) Rounded, sharp, very-sharp and spheroidal (from the left to right)

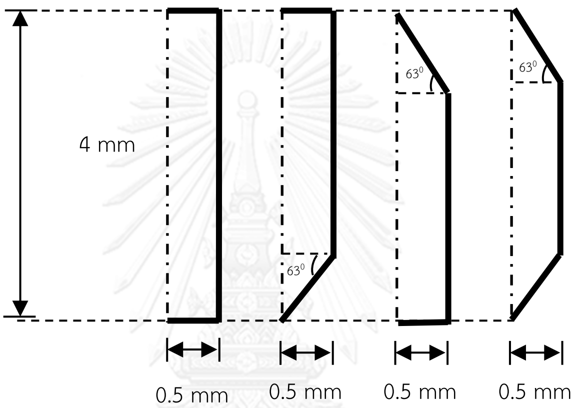

(b) F-F, F-S, S-F, and S-S particles (from the left to right)

Figure 5.2 Particle contours used for (a) standing and (b) floating-particle configurations.

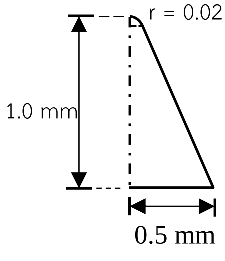

(a) Sharp-tip

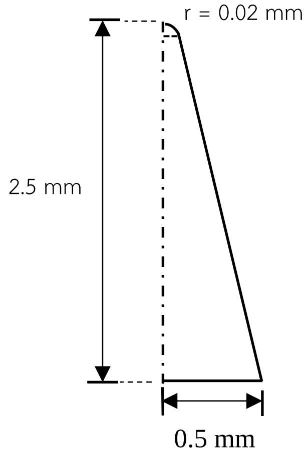

(b) Very-sharp

Figure 5.3 Curvatre at the sharp and very-sharp particle tips of the particles.

5.1.2 Calculation of corona inception voltage

The breakdown criteria (1.1) is widely used to predict breakdown voltage in nonuniform electric field. An equation often used for calculating ionization coefficient is

$$\frac{\bar{\alpha}}{p_1} = 186\left(\frac{E}{p_1} - 2.39\right)^2 \tag{5.1}$$

where E is electric field (kV/mm), p_1 is atmospheric pressure (bar).

Another set of two equations are used for separated ranges of electric field [32]. For 2.588 < E < 7.943 kV/mm,

$$\bar{\alpha} = Cp\left(\frac{E}{p} - \frac{E_M}{p}\right)^2 - Ap \tag{5.2}$$

where p is the pressure (bar) at 20 C$^\circ$, E_M/p, A and C are constant values, equal to 2.165 (kV/mm bar), 0.2873 (1/mm bar) and 1.6053 mm bar/ (kV)^2, respectively. For 7.943 < E < 14 kV/mm,

$$\bar{\alpha} = C_1 E - A_1 p \tag{5.3}$$

where A_1 and C_1 are equal to 80.0006 (1/mm bar), and 16.7766 (1/kV), respectively. Note that for the electric field higher than 14 kV/mm, I also use equation (5.3) to calculate the ionization coefficient. Equations (5.1), (5.2) and (5.3) are applicable to dry air (0 g/m^3 humidity). According to IEC-60052, discharge inception voltage calculated by using these equations increases 0.2% per g/m^3 of humidity [33]. The typical humidity condition is 20 g/m^3 in our experiments. I suppose that calculated discharge inception voltage in the experimental environments increases around 5% from the calculated value.

A method similar to the trapezoidal rule is used to approximate the integration in equation (1.1). The electric field is taken on the axis of symmetry from a particle tip to the upper or grounded electrode. For evaluating the equation numerically, we divide x_c into N intervals and write

$$\int_0^{x_c} \bar{\alpha}\, dx = \sum_{i=1}^{N} \bar{\alpha}_i \, \Delta x_i \tag{5.4}$$

where Δx_i is the width of the i-th subinterval and x_i is the position (Z) at the interval as shown in Figure 5.4. $\bar{\alpha}$ is calculated from equation (5.1) or from equations (5.2) and

(5.3) by using $E = E(x_i)$. Up to 6000 subintervals are used in the calculation. We increase electric field by increasing voltage on the upper electrode until the condition of criteria K in equation (1.1) is satisfied. Therefore, the inception voltage U_i is determined.

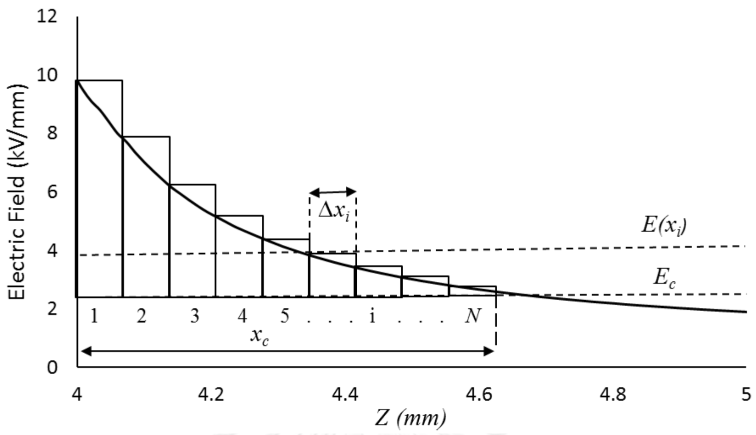

Figure 5.4 Illustration of trapezoidal rule.

5.1.3 Calculated U_i using 3D and AS models with different mesh sizes

The electric field is an important parameter for calculating ionization or corona inception voltage. When the mesh size varies in the model, the calculated U_i also changes due to the accuracy of field computation. This section clarifies the effects of the different mesh sizes and the equations used for calculating ionization on the calculated U_i for the model of standing configuration.

The mesh sizes ranging from 0.0002 to 0.1 mm are used on the particle contour and axis of symmetry to simulate electric field E. The sharp-tip particle shown in Figure 5.2(a) is simulated with an AS model. Figure 5.5 shows the AS sharp-tip particle contours with mesh size of 0.1, 0.01 and 0.001 mm. Figure 5.6 shows the electric field E from axis of symmetry of the AS sharp-tip particle for the mesh sizes from 0.0002 to 0.1 mm. The vertical axis presents the electric field, and the horizontal axis presents the position from the particle tip to the upper electrode. The tendency of E is not much different when the mesh size decreases from 0.001 to 0.0002 mm. Figure 5.7 shows the calculated U_i using equation (5.1), or equations (5.2) and (5.3) with different mesh sizes. The gray solid line presents the experimental value. The dot lines present the calculated U_i using equation (5.1), and black solid lines present the calculated U_i using equations (5.2) and (5.3). From the figure, the calculated U_i decreases with increasing mesh size. For K ranging from 8 to 20, the calculated U_i using equation (5.1) is much lower than the measured U_i due to the high electric field region. The measured U_i is in range of the calculated U_i using equations (5.2) and (5.3) for K from 8 to 20. The calculated U_i using equations (5.2) and (5.3) for K = 9.15 is close to the experimental value.

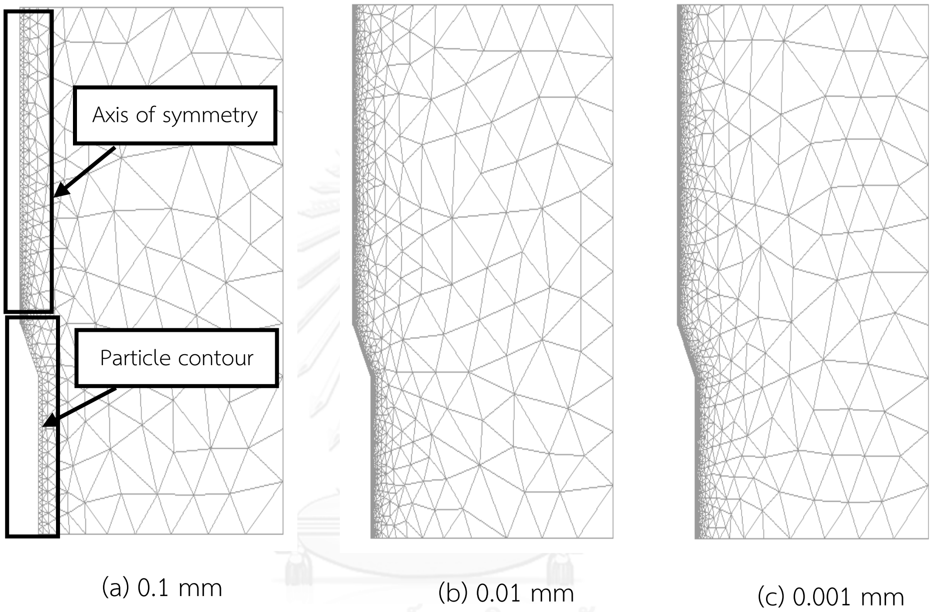

Figure 5.5 Sharp-tip particle in AS model with mess sizes of 0.1, 0.01 and 0.001 mm.

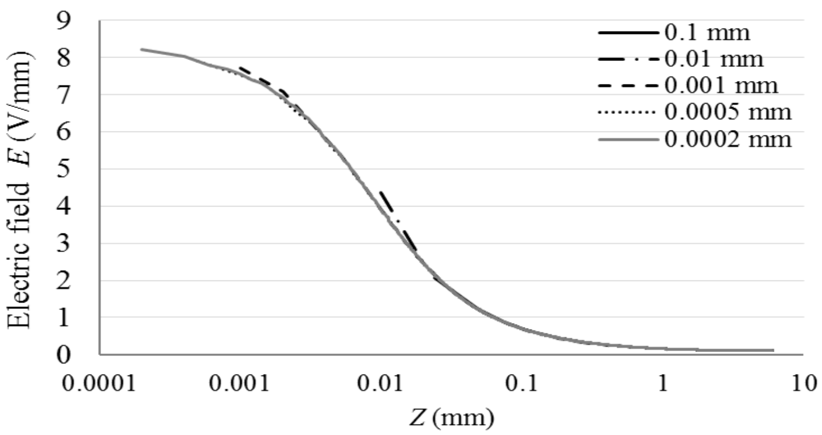

Figure 5.6 Electric field given from axis of symmetry for AS sharp-tip particle for different meh sizes.

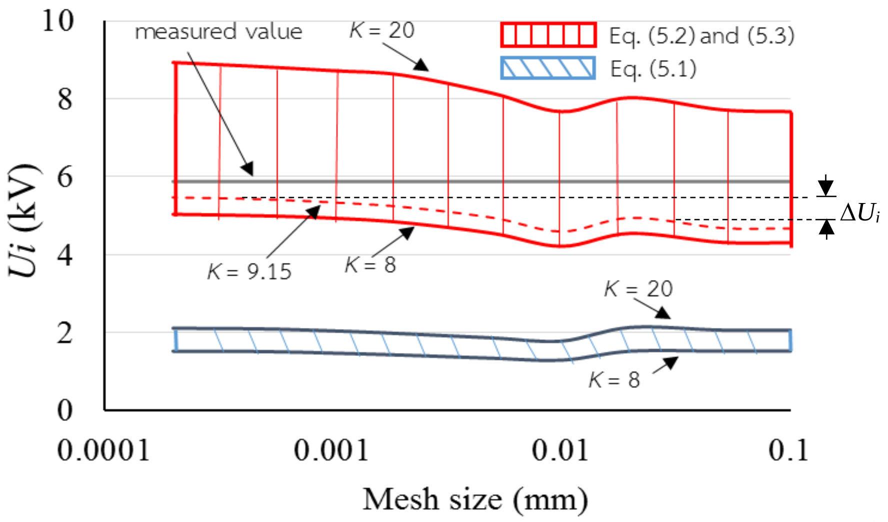

Figure 5.7 Calculated U_i of the sharp-tip particle using the AS model as a function of mesh size (with humidity factor correction).

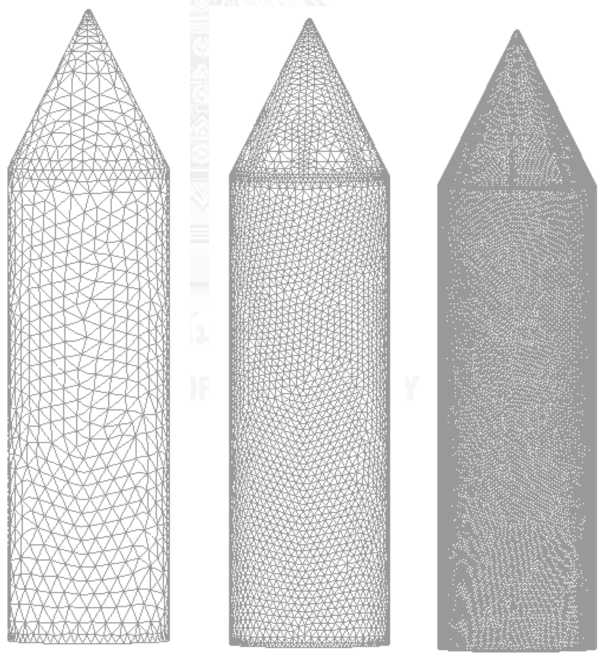

(a) 0.1 mm (b) 0.05 mm (c) 0.02 mm

Figure 5.8 Conical-tip particle in 3D model with mess sizes of 0.1, 0.05 and 0.02 mm.

In order to examine the accuracy of calculated U_i using 3D model, the AS sharp-tip results from the same geometry with mesh sizes from 0.02–0.1 mm are used for comparison. Figure 5.8 shows the 3D particle contours with mesh size of 0.1, 0.05 and 0.02 mm. Figure 5.9 compares the electric field $\boldsymbol{E}$ from the 3D model with that from the AS model. The tendency of E is almost the same for these mesh sizes. Figure 5.10 shows the calculated U_i using equations (5.2) and (5.3) with criteria K = 9.15. The calculated U_i of the 3D and AS models are almost the same for mesh size from 0.02 to 0.1 mm. Anyhow, Figure 5.7 shows that the calculated result using mesh size of 0.02 mm is not accurate enough. Therefore, we expect considerable error by the 3D results due to the limitation of the possible mesh size for calculation.

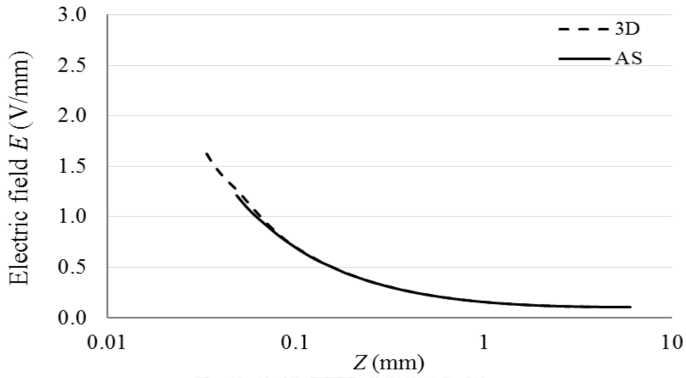

(a) 0.1 mm

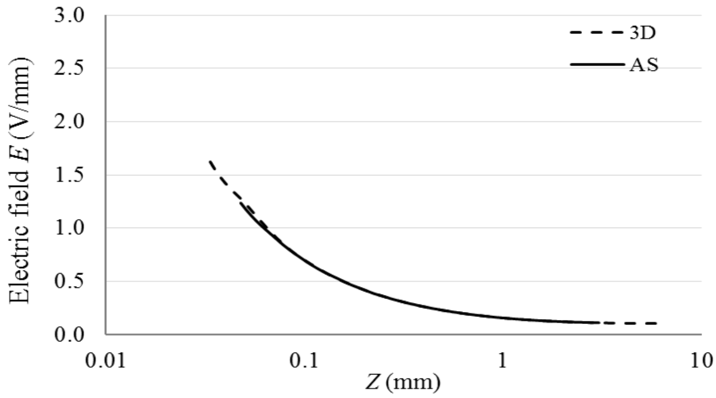

(b) 0.05 mm

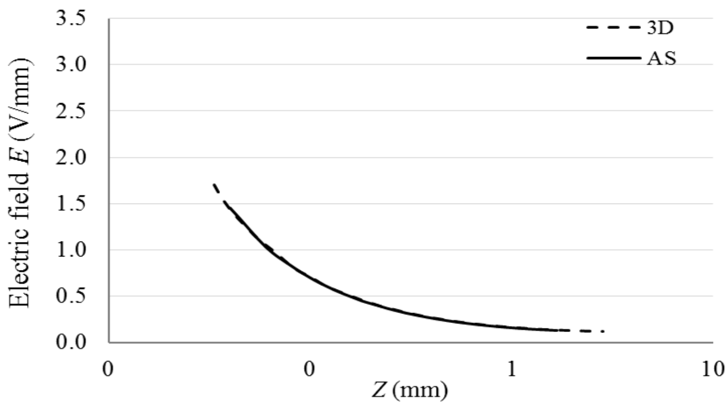

(C) 0.02 mm

Figure 5.9 Electric field from 3D and AS particles.

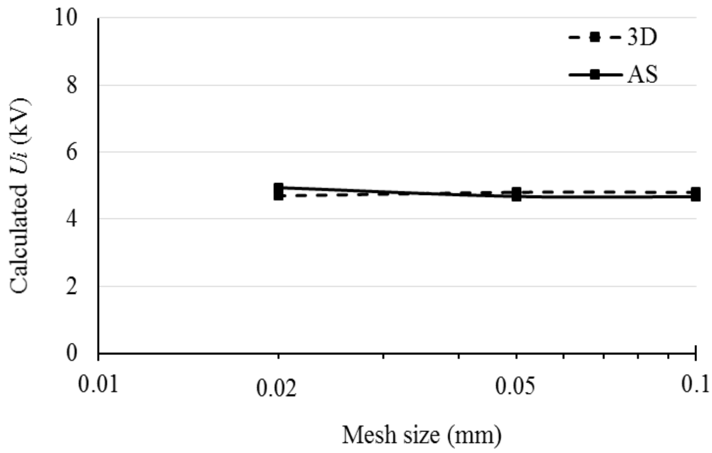

Figure 5.10 Calculated U_i of 3D conical-tip and AS sharp-tip particles using equations (5.2) and (5.3) with N_{cr} = 9.15.

Figure 5.11 shows the 3D model of the sharp-tip particle. Figure 12 shows the 3D particle contours with the same shape of actual particle in Figure 3.5(b). Mesh sizes of 0.1, 0.05 and 0.02 mm are used on the particle contours. Figure 5.13 compares the calculated U_i of the conical-tip and with that of the sharp-tip particles from the 3D models. The electric field on the black dashed line from the particle tip to the upper electrode in Figure 5.11 is used for calculating U_i. Equations (5.2) and (5.3) with K = 9.15 are used. The figure shows that the calculated U_i of the conical-tip particle is lower than that of the sharp-tip particle by about 23%.

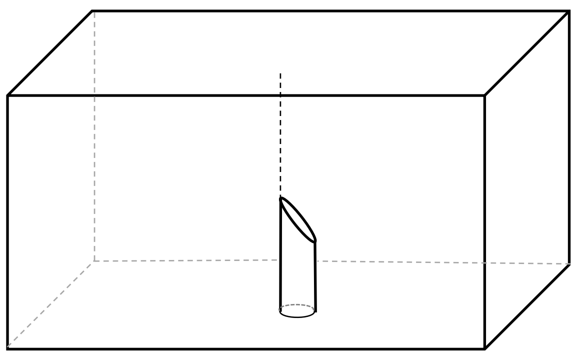

Figure 5.11 3D model of sharp-tip particle

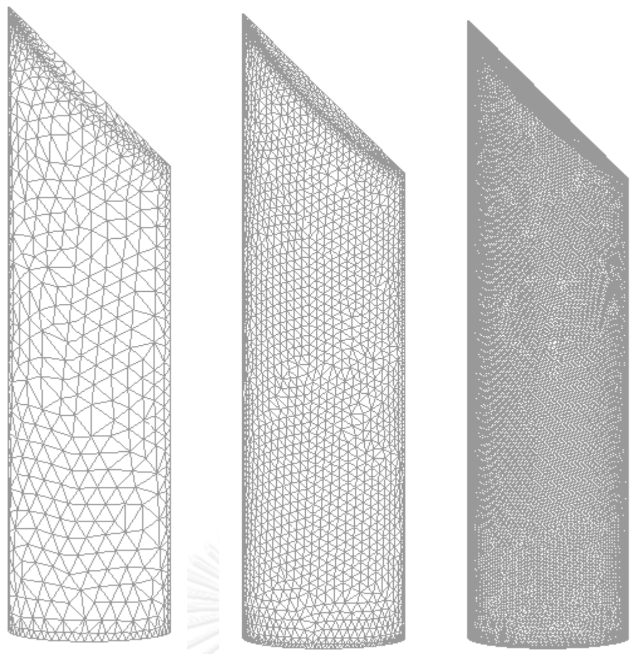

Figure 5.12 Sharp-tip particle in 3D model with mess sizes of 0.1, 0.05 and 0.02 mm.

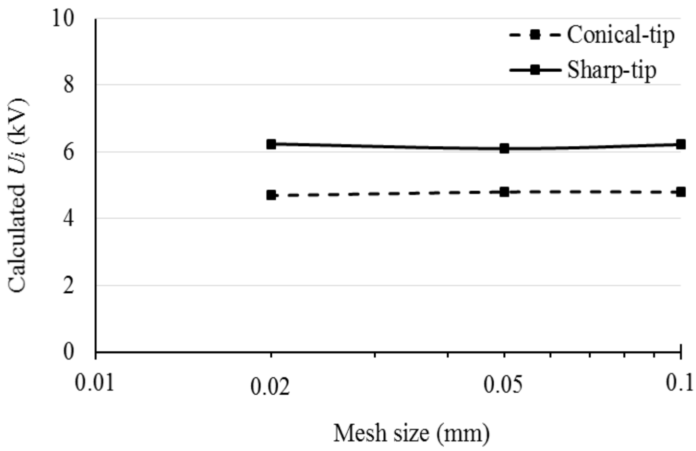

Figure 5.13 Calculated U_i of the 3D conical-tip and the sharp-tip particles using equations (5.2) and (5.3) with K = 9.15.

5.2 Calculation results of the standing particles

The calculation in this section uses the AS model, shown in Figure 5.2(a) and uses equations (5.2) and (5.3) with K = 9.15 for determining U_i. The mesh size is 0.001 mm.

5.2.1. Electric field

Figure 5.14 shows the calculated electric field under a unit applied voltage for different standing particle profiles. The field is given on the axisymmetric line from the particle tip to the upper electrode. Z is the position from the upper tip of the particle to the upper electrode. It is clear that the electric field is highly nonuniform. The maximal electric field is at the particle tip, and the field decreases rapidly with increasing distance from the tip. The particle with a very-sharp tip has the highest field maximum, and the rounded-tip particle has the lowest field minimum.

5.2.2 Calculated U_i

The calculated U_i values of standing particles are shown in Figure 5.15. For the wire particles, the rounded-tip particle has the highest calculated U_i, and the very-sharp tip particle has the lowest calculated U_i. The calculated U_i of the spheroidal particle is between those of the rounded and sharp tip particles. This implies that the lower calculated U_i is heavily influenced by high electric field around the particle tip.

Figure 5.15 also compares the measured results with the calculated U_i. It can be seen that the calculated U_i follows the same tendency as the measured one. The difference ΔU_i (%) can be calculated by

$$\Delta U_i(\%) = \frac{U_{i,cal} - U_{i,meas}}{U_{i,cal}} \times 100 \tag{5.5}$$

where $U_{i,cal}$ and $U_{i,meas}$ are obtained from the calculation and the measurement, respectively. Figure 5.16 shows ΔU_i. The calculated U_i follows the same tendency of the measured U_i. The very-sharp tip particles has the largest difference between the calculated and the measured U_i. The spheroidal particle has smaller ΔU_i than the wire particles. The axisymmetric approximation is one of causes of the difference between the experiments and the analysis. The geometrical difference between the models and the actual particle profiles are significant for the sharp and very-sharp tip particles.

Using actual particle profile for very-sharp and sharp-tip would give higher calculated U_i, as illustrated in section 5.13.

5.2.3 Calculated particle charge

The particle charge Q_{par} before the partial discharge can be calculated by integrating the electric flux density over the particle surface.

$$Q_{par} = \oint \varepsilon_0 E ds \tag{5.6}$$

where E is electric field, S is particle surface and $\varepsilon_0 = 8.854 \times 10^{-12}$ F/m, permittivity of free space.

Figure 5.17 shows the calculated particle charge Q_{par} and the measured PD charge Q_{PD} for the standing particles. The Q_{PD} charge is measured from R_m = 50 Ω. It can be seen that the tendency of Q_{par} follows the same tendency of PD charge Q_{PD}. Figure 5.18 plots PD charge versus the particle charge. The upper and lower bars present the maximal and minimal of the measured PD charges, respectively. The PD charge varies more or less linearly with the calculated particle charge.

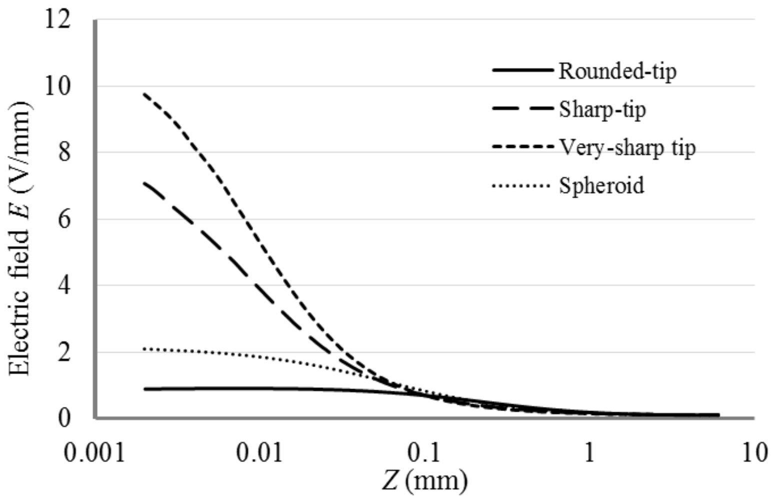

Figure 5.14 Electric field along axis of symmetry for the standing particle tips under 1-V application.

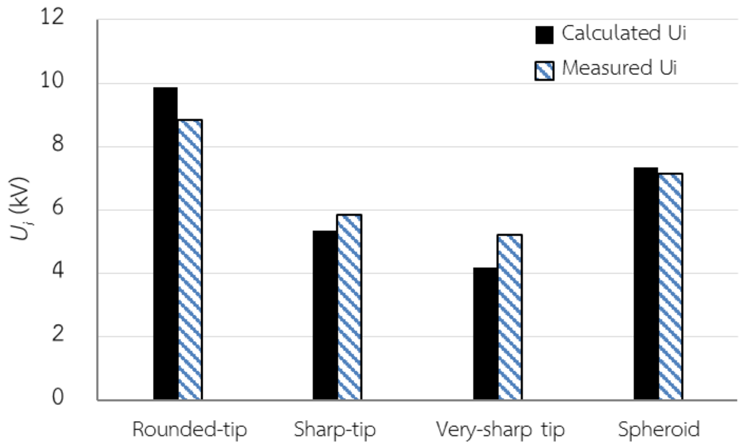

Figure 5.15 Calculated corona inception voltage for the standing particles.

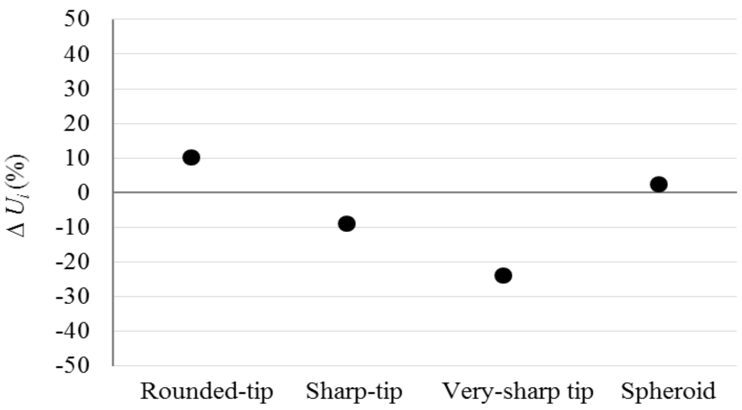

Figure 5.16 Difference between the measured and the calculated corona inception voltages for the standing particles.

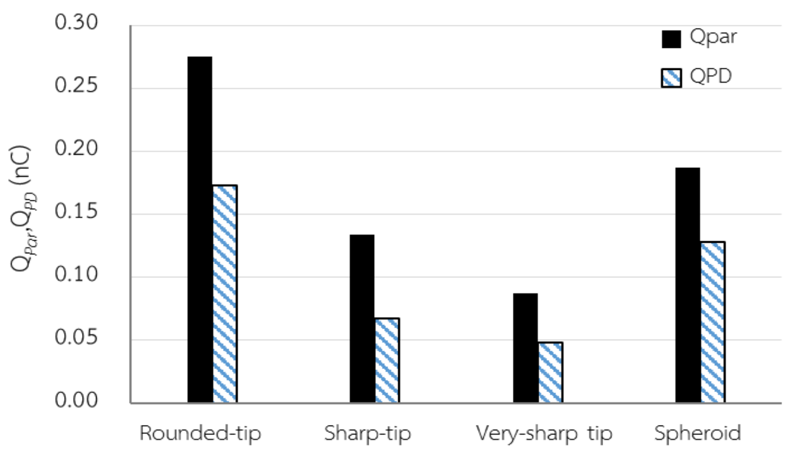

Figure 5.17 Calculated particle charge and PD charge for the standing particles.

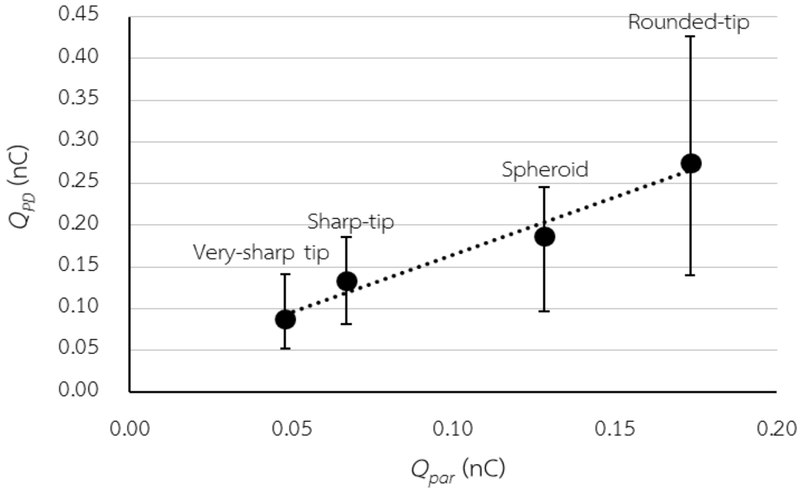

Figure 5.18 Comparison of PD charge and particle charge for the standing particles.

5.3 Calculation results of floating particles

The calculation in this section uses the AS model, shown in Figure 5.2(b) and uses equations (5.2) and (5.3) with K = 9.15 for determining U_i. The mesh size is 0.001 mm.

5.3.1 Electric field

Figure 5.19 and 5.20 show the electric field along the axis of symmetry for the floating particles at both upper and lower gaps. For the horizontal axis, Z is the position from the upper particle tip to the upper electrode for the left graphs, and from the lower particle tip to the grounded electrode for the right graphs. The maximal electric field is at the sharp tip of particle. For the particle having the same two shape tips, the electric field at the lower tip is higher than that at the upper tip for smaller gap. The field is almost the same at both tips for larger gap from 1 to 2 mm. The electric field at both tips increase with increasing gap at small gap, but they hardy vary with increasing gap for larger gap.

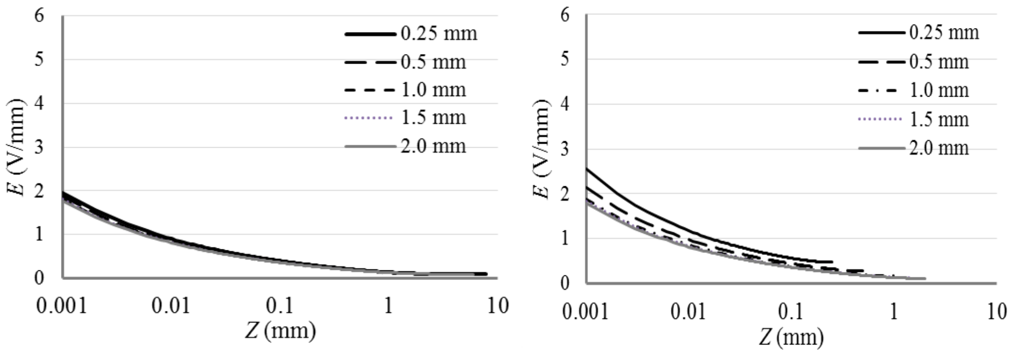

(a) F-F particle

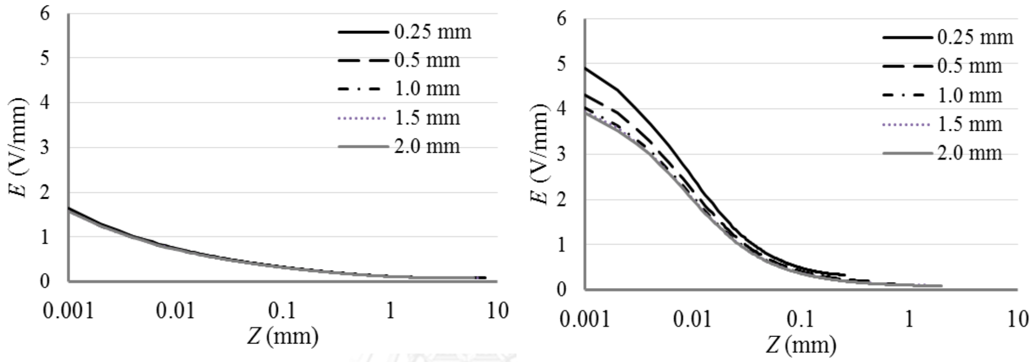

(b) F-S particle

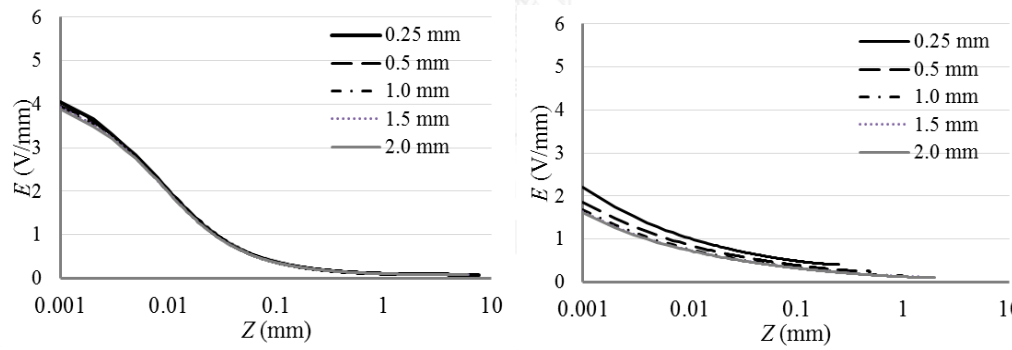

(c) S-F particle

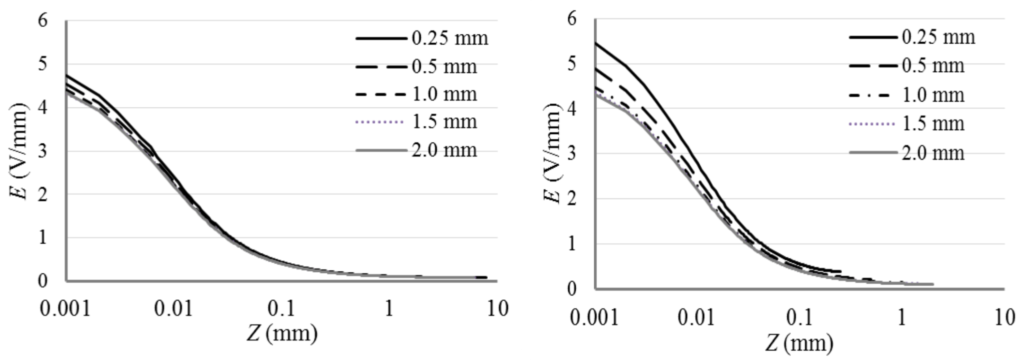

(d) S-S particle

Figure 5.19 Electric field at the upper (left graphs) or lower (right graphs) gaps as a function of gap lengths for the floating particles.

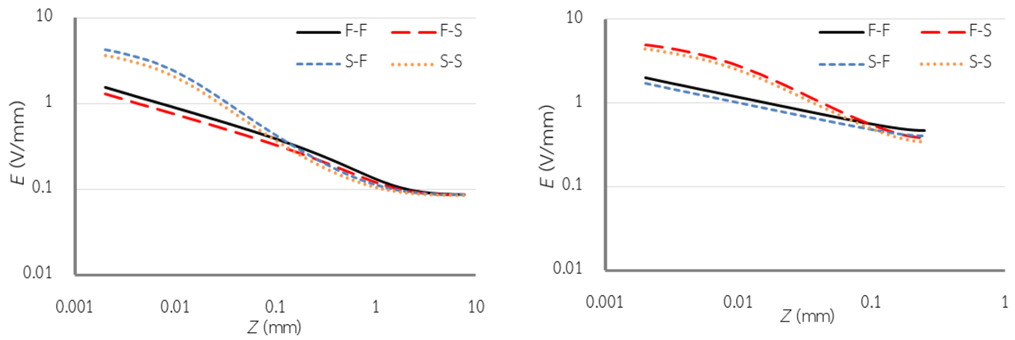

(a) g = 0.25 mm

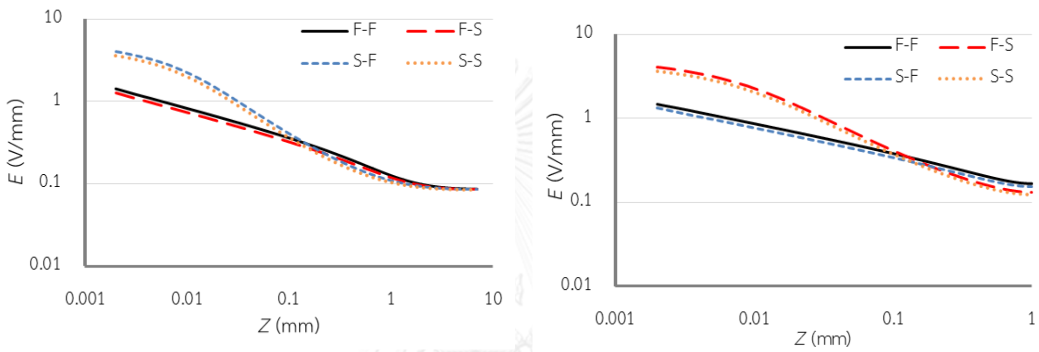

(b) g = 1.0 mm

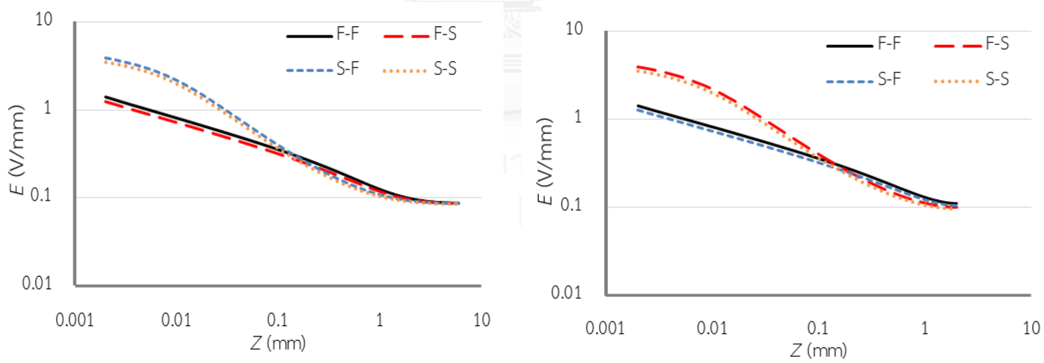

(c) g = 2.0 mm

Figure 5.20 Electric field on the upper (left graphs) or lower (right graphs) gaps as a function of particle profile for the floating particles.

5.3.2 Calculated U_i

For the floating particles, the calculated U_i is determined as the voltage by which the discharge takes place both the upper and the lower gaps. For the F-F and S-S particles, the calculation results show that the discharge takes place at both upper and lower gaps almost at the same voltage at g from 1 to 2 mm. Therefore, the inception voltage is determined from a single calculation process. For F-F and F-S in the case g = 0.25 and 0.5 mm, the calculation procedure follows the procedure of the F-S particle. For the F-S particles, the discharge condition is initially satisfied at the lower gap for all gap lengths with the particle potential $U_p = U_{p0}$. We assume that U_{p0} decreases by δU because of loss of positive charge after initial discharge at the lower gap. The particle potential decreases by

$$U_p = U_{po} - \delta U \tag{5.7}$$

$$0 \le \frac{\delta U}{U_{p0}} \le 1 \tag{5.8}$$

.

After that, if a discharge condition is not satisfied at the upper gap between the particle and the upper electrode, the applied voltage at the upper electrode is increased until the condition is satisfied. The calculation procedure is shown in Figure 5.21. Figure 5.22 shows the calculated U_i at the upper as a function of gap length for different $\delta U / U_{p0}$. The calculated U_i of the F-S particle increases with increasing $\delta U / U_{p0}$ or gap lengths.

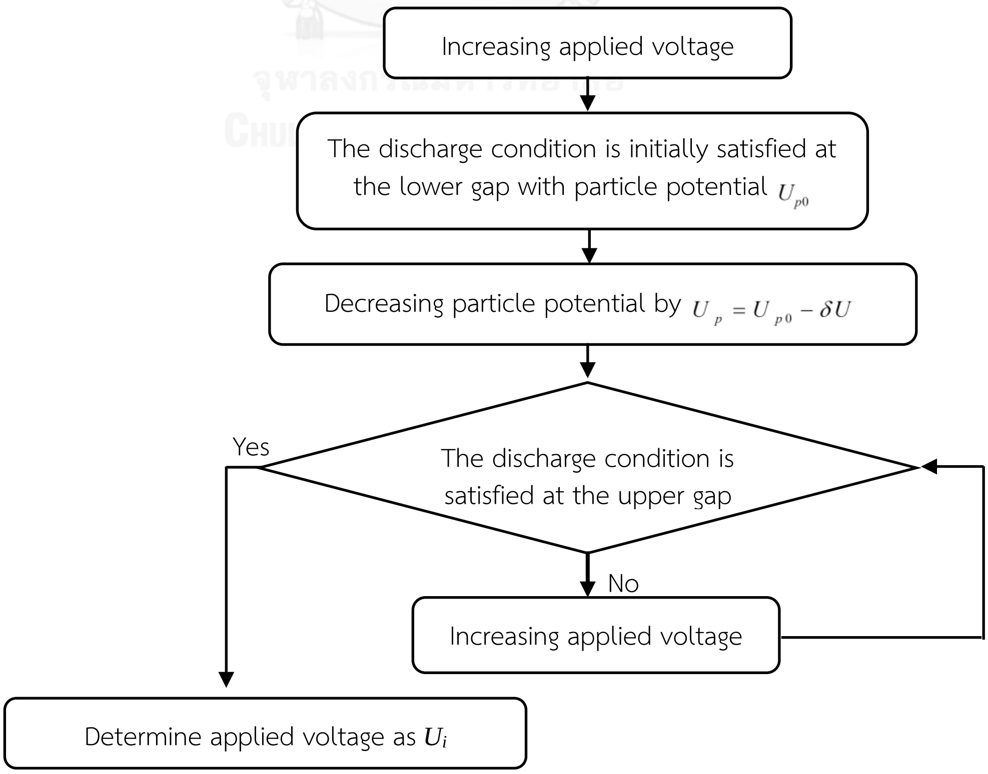

Figure 5.21 Flowchart of calculating U_i procedure of the F-S particles.

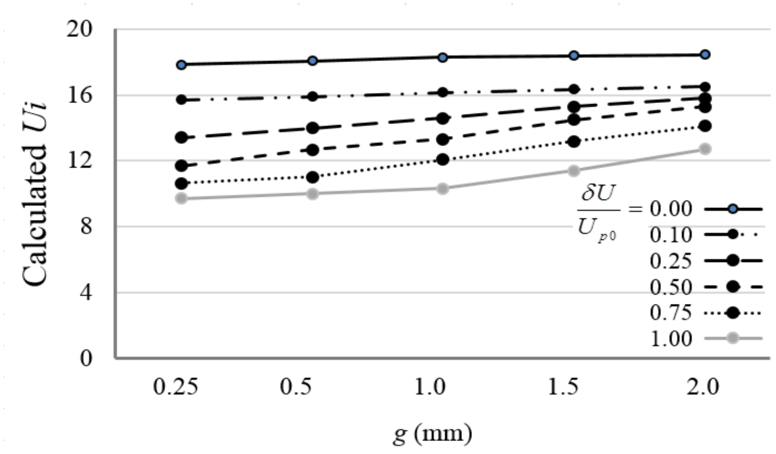

Figure 5.22 Calculated U_i of the F-S particle as a function of gap length.

For the S-F particle, the discharge condition is initially fulfilled at the upper gap. We assume the particle potential increases from U_{p0} to U_{app0} (applied voltage of the initial discharge at the upper gap) due to loss of negative charge. The particle potential increases by

$$U_p = U_{p0} + \delta U \tag{5.9}$$

$$0 \leq \frac{\delta U}{U_{app0} - U_{p0}} \leq 1 \tag{5.10}$$

The particle is fixed at this value. If discharge condition is satisfied at the lower gap, then the calculated U_i is determined at this voltage. If the discharge condition is not satisfied, the applied voltage is increased until the condition is satisfied. The calculation procedure of the S-F particle is shown in Figure 5.23. Figure 5.24 shows the calculated U_i of the S-F particle at the lower gap as a function of gap length for different $\delta U / (U_{app0} - U_{p0})$. From the figure, the calculated U_i increases with increasing gap. For $\delta U / (U_{app0} - U_{p0})$ from 0.25 to 1, the discharge condition is satisfied at both upper and lower gaps. Therefore the lines from 0.25 to 1 are merged together. Anyhow, the calculation scheme does not give a reasonable results for the F-S and S-F particles. This may be because of the particle potential is not updated with the increasing of the applied voltage.

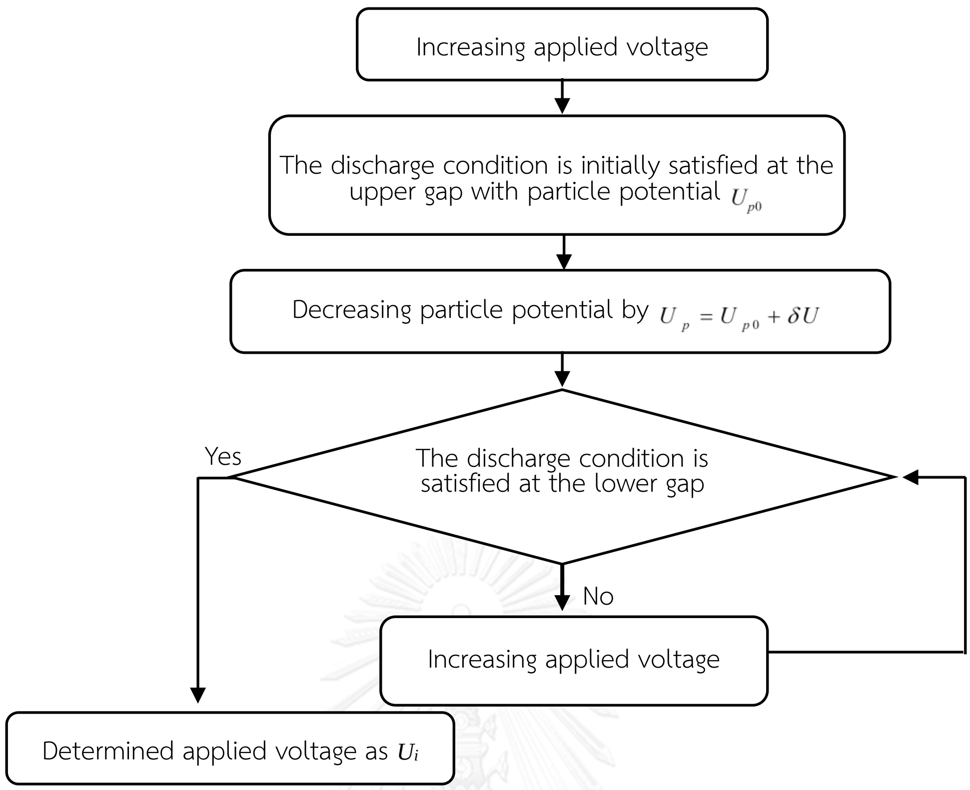

Figure 5.23 Flowchart of calculating U_i procedure of the S-F particles.

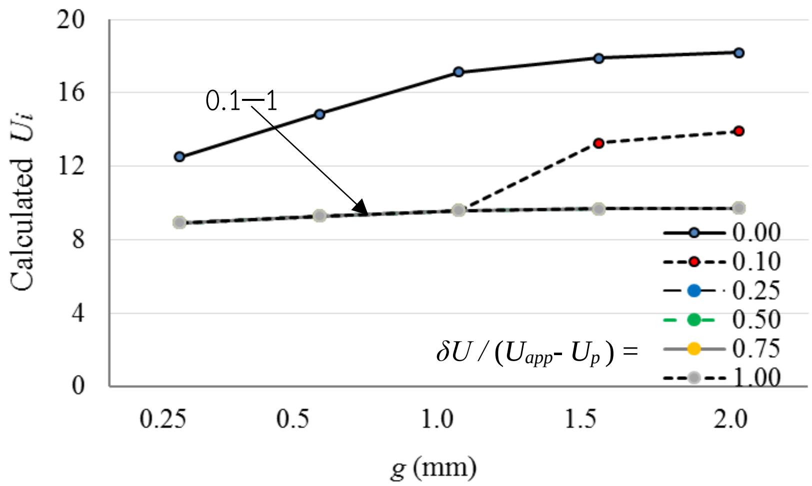

Figure 5.24 Calculated U_i of the S-F particle as a function of gap length.

The following results are calculated by using $\delta U / U_{p0}$ or $\delta U / (U_{app0} - U_{p0})$ = 0.1, which is small adjustment of U_{p0} for the floating particles. Figure 5.25 shows the calculated U_i with 0.1 adjustment of U_{p0} as a function of gap lengths for the floating particles. The calculated U_i of the F-F and F-S particle slightly increases with increasing g = 0.25–2.0 mm.

For the S-F particle, the calculated U_i is more or less constant with increasing g from 0.25 to 1 mm, and increases with increasing g (1.0 to 2.0 mm). The tendency of the calculated U_i of the S-F particle is different from the measured value where the measured U_i decreased with increasing g from 1.0 to 2.0 mm. That is caused by estimation of particle potential after initial discharge at the upper gap. For S-S particle, the calculated U_i increases with increasing g from 0.25 mm to 1.0 mm, and keeps constantly with increasing g from 1 to 2 mm. Figure 5.26 shows the calculated U_i as a function of particle profiles. The flat upper tip effects on the calculated U_i as the calculate U_i of the F-F and F-S particle with the flat upper tips are higher than those of particle having sharp upper tip for all gap lengths.

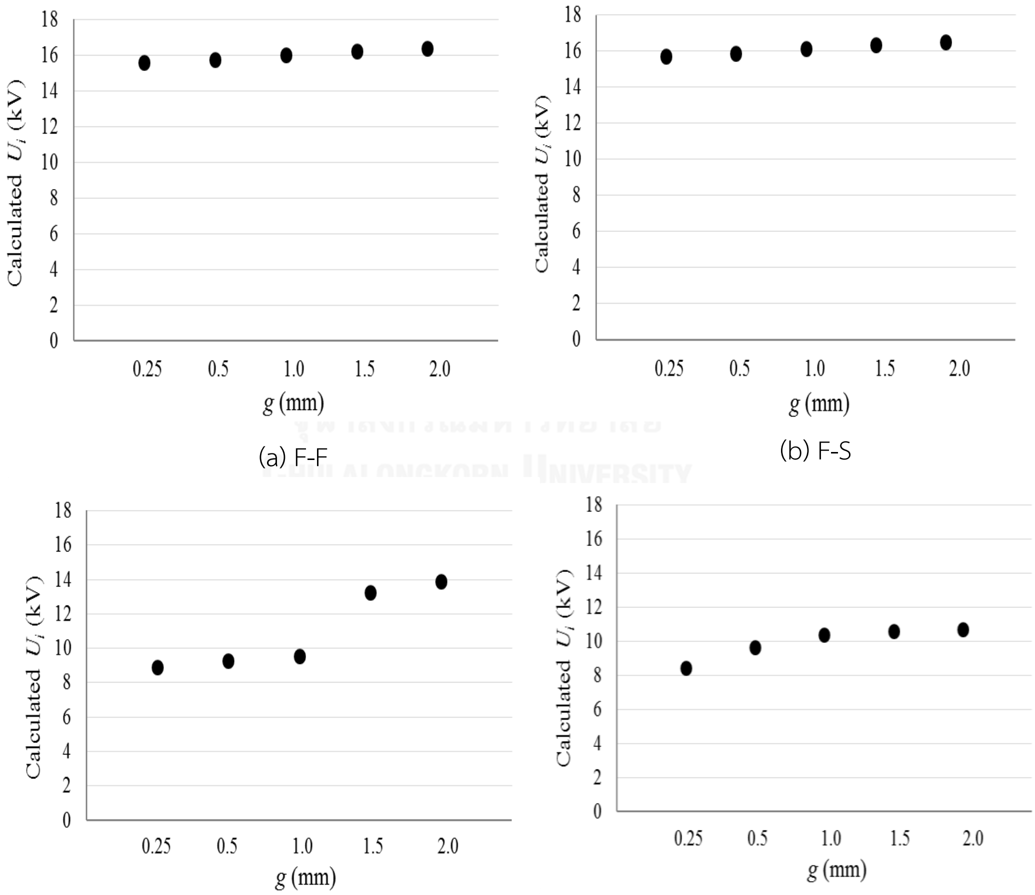

(a) F-F

(b) F-S

(c) S-F

(d) S-S

Figure 5.25 Calculated U_i as a function of gap lengths for the floating particles.

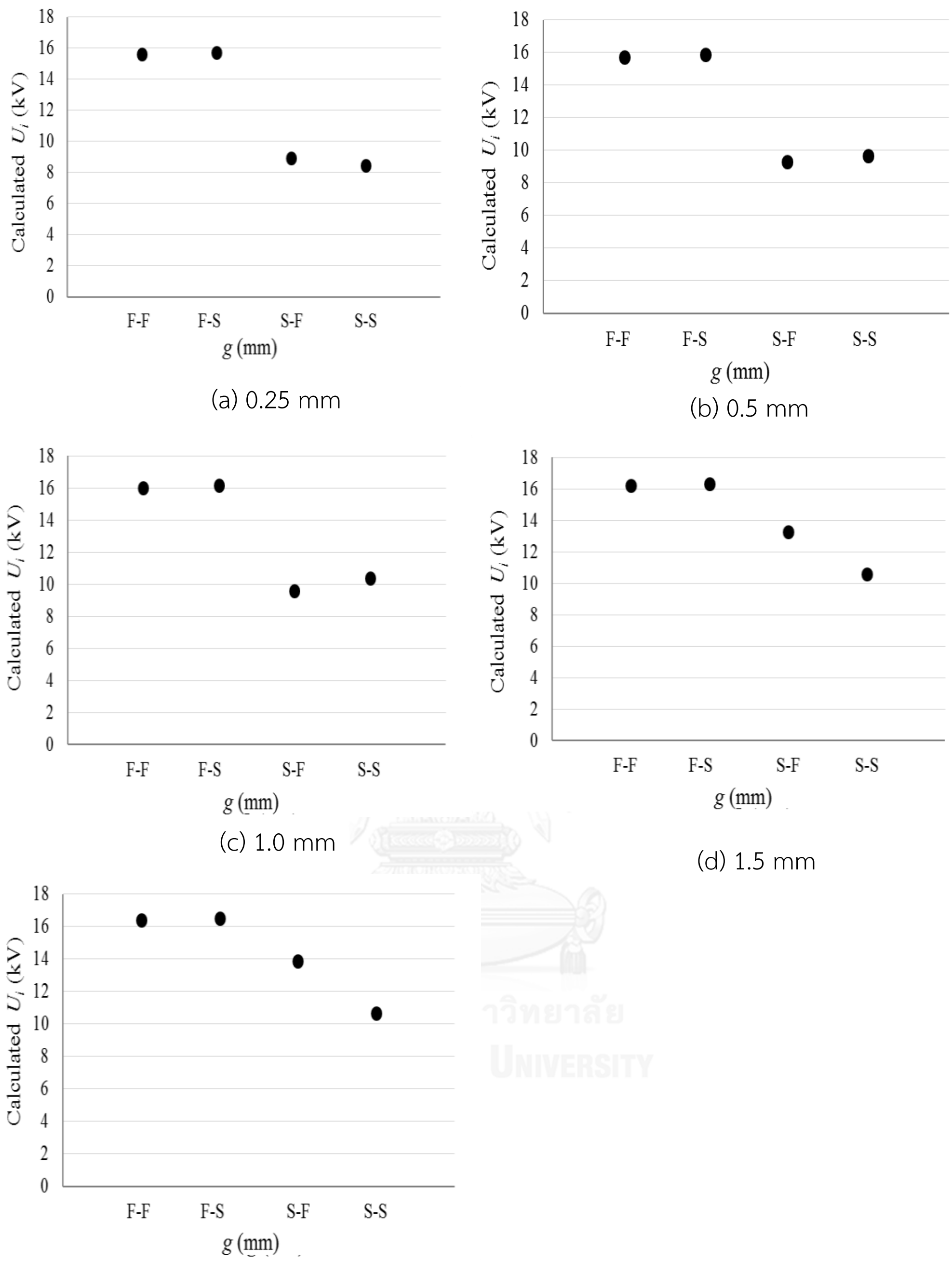

(a) 0.25 mm

(b) 0.5 mm

(c) 1.0 mm

(d) 1.5 mm

(e) 2.0 mm

Figure 5.26 Calculated U_i as a floating particle profile.

CHAPTER VI
CONCLUSIONS

6.1 Experimental results

For the standing particles, the corona inception voltage and PD charge measured from 50 and 500 Ω R_m are not much different from each other. The corona inception voltage is lower with sharper particle tip. PD charge follows the tendency of the corona inception voltage. The current magnitude is higher for the case 50 Ω than for the case 500 Ω.

For the floating particles, the particles having flat upper tips yield direct breakdown for smaller gap and corona discharge for larger gap. The particles having sharp upper tips exhibit corona for all gap lengths. The corona inception voltage of the particles having sharp upper tips increase with increasing gaps from 0.25 to 1.0 mm, but decrease from 1.0 to 2.0 mm. the corona inception voltage of the particle having flat upper tips are higher than those of the particle having sharp lower tips. For the particles having the same upper tips, the sharp lower tip exhibits lower corona inception than that for flat lower tip. The PD charges do not follow the tendency of corona inception voltage. The PD charge tended to be lower for smaller gap for all particles.

6.2 Analytical results

The calculated corona inception voltage increases with increasing mesh size from the model. The mesh sizes from 0.001 to 0.0002 mm give high accurate results for AS model. Using actual particle profile for the sharp-tip particle gives higher calculated corona inception voltage than that using axisymmetric approximation.

For the standing particles, the electric field on the upper particle tips mainly determined the calculated U_i. The calculated corona inception voltage follows the tendency of the measured values. The very-sharp tip particle has the largest different between the calculated and measured values. The tendency of calculated particle charge follows tendency of PD charge. The PD charge varies more or less linearly with the calculated particle charge.

For the floating particles, U_i depended on the mechanics of the discharge at the upper and lower particle tips. The calculated U_i did not agree well with the measured ones. This may be due to the inappropriate assumption of particles potential and the influence of space charges on the field distribution.

REFERENCES

[1] A. Sabat and S. Karmakar, "Simulation of Partial Discharge in High Voltage Power Equipment," *International Journal on Electrical Engineering and Informatics,* vol. 3, pp. 234-247, 2011.

[2] IEEE Power & Energy Society, "IEEE guide for Sulphur Hexafluoride (SF6) gas handling for high-voltage (over 1000 Vac) equipment," IEEE, pp. 1-69, 2011.

[3] D. B. Durocher, M. Haim, L. T. Connor, and J. d. Jong, "Safety by design: Solid insulated technologies challenge the use of SF6 in medium-voltage switchgear," Proc. *2015 IEEE IAS Electrical Safety Workshop*, pp. 1-9, 2015.

[4] J. D. McDonal, "Electric power substations engineering," *CRC Press,* 2012.

[5] D. V. Yamille, H. Nigel, J. Perkel and R. Cary, "Underground cable systems," *Springer Science+ Business Media,* 2012.

[6] S. A. Ward, A. A. Elfaraskoury, S. S. Elsayed, "Experimental and theorytical study of breakdown voltage initiated by particle contamination in GIS," *International Journal of Scientific Research Engineering & Technology (IJSRET),* vol. 3, pp. 241-247, 2014.

[7] T. Takuma and B. Techaumna, "*Electric fields in composite dielectrics and their applications,"* Springer, 2010.

[8] I. R. Velo, "Experimental set-up for partial discharge detection," Master thesis, Department of Electrical Power Engineering, Norwegian University of Science and Technology, NTNU, 2015.

[9] M. M. A. Refaey, "Factors of influence on the erosion of epoxy resin insulating material by corona discharges," Ph.D thesis, Department of Electrical and Computer Engineering, Technical University of Munich, 2014.

[10] T. Berg, M. Zamani, M. Muhr, and D. Imamovic, "Investigations of conductive particles in gas insulated Systems under DC-conditions," *Proc. conference on Electrical Insulation and Dielectric Phenomena*, pp. 1000-1003, 2013.

[11] V. Q. Huynh, B. Techaumnat, and K. Hidaka, "Analysis on electrostatic behavior of a conducting prolate spheroid under an electric field," *IEEE Trans. on Dielectrics and Electrical Insulation,* vol. 20, pp. 2230-2238, 2013.

[12] K. I. Sakai, D. L. Abella, Y. Khan, J. Suehiro, and M. Hara, "Theoretical and experimental studies for spherical free-conducting particle behavior between nonparallel plane electrodes with AC voltages in air," *IEEE Trans. on Dielectrics and Electrical Insulation,* vol. 10, pp. 404-417, 2003.

[13] Y. Kudo, T. Sugimoto, and Y. Higashiyama, "DC corona discharge from a wire particle floated with a microgap in parallel plate electrodes," IEEE Trans. on *Industry Applications*, vol. 42, pp. 909-915 ,2006.

[14] K. Asano, R. Hishinuma, and K. Yatsuzuka, "Bipolar DC corona discharge from a floating filamentary metal particle," IEEE Trans. on *Industry Applications, vol. 38, pp 57-63.2002.*

[15] Y. Negara, K. Yaji, J. Suehiro, N. Hayashi, and M. Hara, "DC corona discharge from floating particle in low pressure SF6," *IEEE Trans. on Dielectrics and Electrical Insulation,* vol. 13, pp. 1208-1216, 2006.

[16] M. M. Morcos, H. Anis, and K. D. Srivastava, "Particle-initiated corona and breakdown in GITL systems," *IEEE Trans. on Electrical Insulation,* vol. 24, pp. 561-571, 1989.

[17] M. M. Morcos, S. Zhang, K. D. Srivastava, and S. M. Gubanski, "Dynamics of metallic particle contaminants in GIS with dielectric-coated electrodes," *IEEE Trans. on Power Delivery,* vol. 15, pp. 455-460, 2000.

[18] M. M. Morcos, S. A. Ward, and H. Anis, "On the detection and control of metallic particle contamination in compressed GIS equipment," Proc. conference on *Electrical Insulation and Dielectric Phenomena*, vol. 2, pp. 476-480,1998.

[19] Y. Khan, K. I. Sakai, E. K. Lee, J. Suehiro, and M. Hara, "Motion behavior and deactivation method of free-conducting particle around spacer between diverging conducting plates under DC voltage in atmospheric air," *IEEE Trans. on Dielectrics and Electrical Insulation,* vol. 10, pp. 444-457, 2003.

[20] M. Kubuki, R. Yoshimoto, K. Yoshizumi, S. Tsuru, and M. Hara, "Estimation of dc breakdown mechanisms in air gaps containing floating metallic particles," *IEEE Trans. on Dielectrics and Electrical Insulation,* vol. 4, pp. 92-101, 1997.

[21] H. R. Hiziroglu and S. A. Sebo, "Calculation of breakdown voltages of short air gaps," Proc. conference on *Electrical Insulation and Dielectric Phenomena*, vol. 1, pp. 435-438, 2000.

[22] K. Petcharaks, "A contribution to the streamer breakdown criterion," Eleventh International Symposium on High Voltage Engineering on *High Voltage Engineering, vol. 3,* pp. 19-22,1999.

[23] T. M. P. Briels, J. Kos, G J J Winands, E. M. V. Veldhuizen and U. Ebert, "Positive and Negative Streamers in Ambient Air: Measuring Diameter, Velocity and Dissipated energy," *Applied Physics,* vol. 41, 2008.

[24] V. Q. Huynh, "Study on the electromechanics of non-spherical particles under electric field in dielectric systems," Ph.D thesis, Department of Electrical Engineering, Chulalongkorn University, 2013.

[25] E. Kuffel, W. S. Zaengl, and J. Kuffel, "*High Voltage Engineering",* Springer, 2000.

[26] J. S. Chang, P. A. Lawless, and T. Yamamoto, "Corona discharge processes," *IEEE Trans. on Plasma Science,* vol. 19, pp. 1152-1166, 1991.

[27] T. Plank, "Positive Corona at Combined DC and AC Voltage," Ph.D thesis, Department of Physics, University of Tartu, 2001.

[28] D. Xiao, "*Gas discharge and gas insulation*," Springer, 2016.

[29] M. Aissou, H. Ait Said, H. Nouri, and Y. Zebboudj, "Effect of relative humidity on current–voltage characteristics of monopolar DC wire-to-plane system," *Journal of Electrostatics,* vol. 76, pp. 108-114, 2015.

[30] H. V. P. Nguyen, B. T. Phung, and T. Blackburn, "Effect of temperatures on very low frequency partial discharge diagnostics," IEEE 11th International Conference on the Properties and Applications of Dielectric Materials, pp. 272-275, 2015.

[31] P. K. Panicker, "Ionization of air by corona discharge," Master degree thesis, Department of Aerospace Engineering, The University of Texas at Arlington, 2003.

[32] K. Petcharaks, "Application of the streamer breakdown criterion to inhomogeneouse gas gaps," Ph.D thesis, Swiss Federal Institute of Technology, 1995.

[33] IEC 60052, "Recommendation for voltage measurement by means of sphere-gap (one sphere-earthed)," 1960.

APPENDIX

PD current waveforms

PD current waveforms are detected by an oscilloscope (TDS 754A, 500 MHz, 2 GS/S). 50 Ω and 1 MΩ of input impedance in the oscilloscope are used. The left and right graphs present the PD current waveforms detected by oscilloscope using 50 Ω and 1 MΩ, respectively. The PD current waveforms detected by using input impedance of 50 Ω were smother, but had smaller magnitude than theses using 1 M Ω. This is because with 50 Ω input impedance, the oscilloscope measured only a half of the PD current.

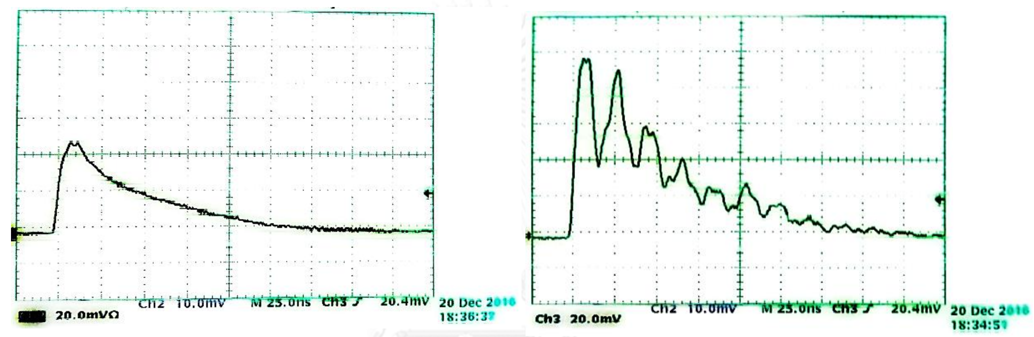

(a) Rounded-tip particle

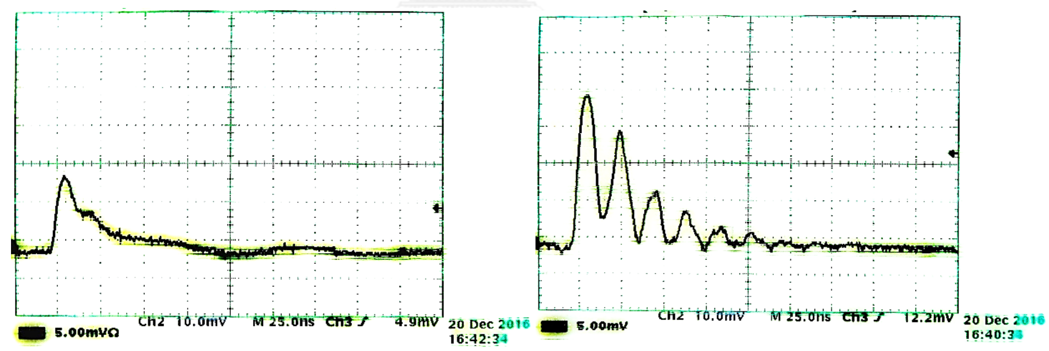

(b) Sharp tip particle

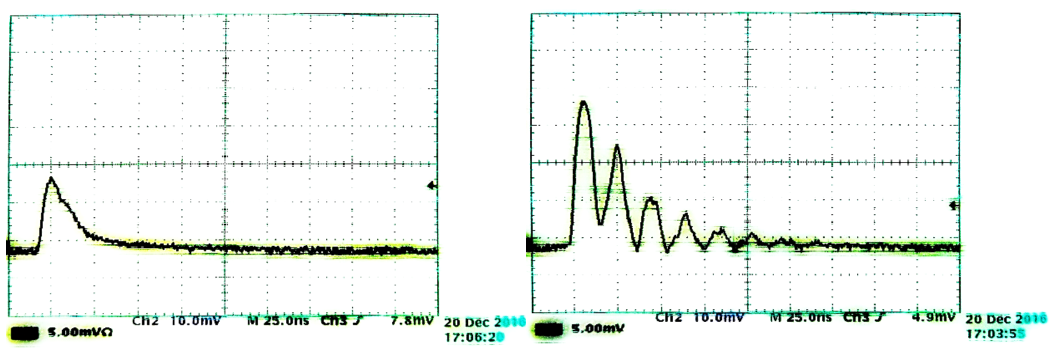

(c) Very-sharp tip particle

Figure A.1 PD current waveforms detected by oscilloscope using input impedancce of 50 Ω (left graphs) and 1 MΩ (right graphs).

VITA

Chomrong Ou was born in 1990, Prey Veng province, Cambodia. He received bachelor’s degree in electrical engineering, department of electrical and energy, Institute of Technology of Cambodia, Phnom Penh, Cambodia. In 2014, he received a scholarship from ASEAN University Network/Southeast Asia Engineering Education Development Network (AUN/SEED-Net) for pursuing master’s degree in electrical engineering, department of electrical engineering, faculty of engineering, Chulalongkorn University, Thailand. His research interest is study on particle-induced corona discharge in insulation systems.